Dr. 199

ERDA/JPL/954144-76/1

SILICON RIBBON GROWTH BY A CAPILLARY ACTION SHAPING TECHNIQUE

Quarterly Technical Progress Report No. 3, March 15, 1976

G. H. Schwuttke
T. F. Ciszek
A. Kran

1976

Work Performed Under JPL Contract No. 954144

East Fishkill Laboratory
International Business Machines Corporation
Hopewell Junction, New York

ENERGY RESEARCH AND DEVELOPMENT ADMINISTRATION
Division of Solar Energy

DISCLAIMER

Printed in the United States of America
USERDA Technical Information Center, Oak Ridge, Tennessee

ERDA/JPL/954144-76/1
Distribution Category UC-63

SILICON RIBBON GROWTH BY A CAPILLARY ACTION SHAPING TECHNIQUE

G. H. Schwuttke, Principal Investigator, 914-897-3140
International Business Machines Corporation
System Products Division, East Fishkill Laboratories
Hopewell Junction, New York 12533

Quarterly Technical Progress Report Number 3
March 15, 1976

prepared by

G. H. Schwuttke, T. F. Ciszek, and A. Kran

Under JPL Contract Number: 954144
(Subcontact under NASA Contract NAS7-100)
(Task Order No. RD-152)

CONTENTS

TECHNICAL CONTENT STATEMENT

This report contains information prepared by the International Business Machines Corporation under JPL contract. Its contents are not necessarily endorsed by the Jet Propulsion Laboratory, California Institute of Technology, or by the National Aeronautics and Space Administration.

RESEARCH PROGRAM PLAN

OBJECTIVES

1. Technological assessment of ribbon growth of silicon by a capillary action shaping technique.

2. Economic evaluation of ribbon silicon grown by a capillary action shaping technique as low-cost silicon.

SYNOPSIS OF PROGRAM OF STUDY

1. Crystal growth of silicon ribbons.

2. Characterization of silicon ribbons.

3. Economic evaluations and computer-aided simulation of ribbon growth.

THIRD QUARTER HIGHLIGHTS

- Ribbons 25 mm wide and 0.5 m long were grown from silicon carbide dies.

- Thermal modifiers were studied, and systems were developed that reduce frozen-in stress in silicon ribbons and improve thickness uniformity.

- Spreading-resistance measurements indicate that resistivity variations of up to 200% are caused by grain boundaries. Twin boundaries give no indication of similar fluctuations in resistivity.

- Electron channeling patterns are applied to analyze surface orientations of ribbons grown with carbon dies.

- Surface orientation of ribbon sections grown under steady-state conditions approaches the <011> direction.

- Single- and double-tilt misalignment off the <011> directions occurs.

- Best ribbons grown show 5 to 8 degrees single tilt in surface orientation off <011> and twin lines in the <112> growth direction.

- Seed orientation has no influence on final surface orientation.

- Technology projection and sensitivity analysis indicate that single-ribbon growth systems--as opposed to multi-ribbon systems--offer the best potential for achieving low-cost silicon sheet material within the shortest period of time.

- Processing-technology improvements are the key elements for reducing cost of silicon sheets.

- Significant reductions in sheet material cost are achievable in the near future by increasing ribbon width to 5 cm.

CRYSTAL GROWTH

by

T. F. Ciszek

1. INTRODUCTION

The crystal-growth method under investigation is a capillary action shaping technique. Meniscus shaping for the desired ribbon geometry occurs at the vertex of a wettable die. As ribbon growth depletes the melt meniscus, capillary action supplies replacement material. The configuration of the technique used in our initial studies is shown in Fig. 1 and is similar to the EFG process described by LaBelle (1). The crystal-growth method has been applied to silicon ribbons for several years (2,3,4), and long ribbons up to 25 mm in width have been produced.

Certain problems still await solution before the technique becomes viable for large-scale economical photovoltaic applications. High-density graphite fulfills the durability and wettability requirements of a die (2) and has been used, to date, for most silicon ribbon growth; it is not, however, completely non-reactive. Good crystallographic perfection has been achieved on small ribbon segments (2,3), but the structure of large ribbons is

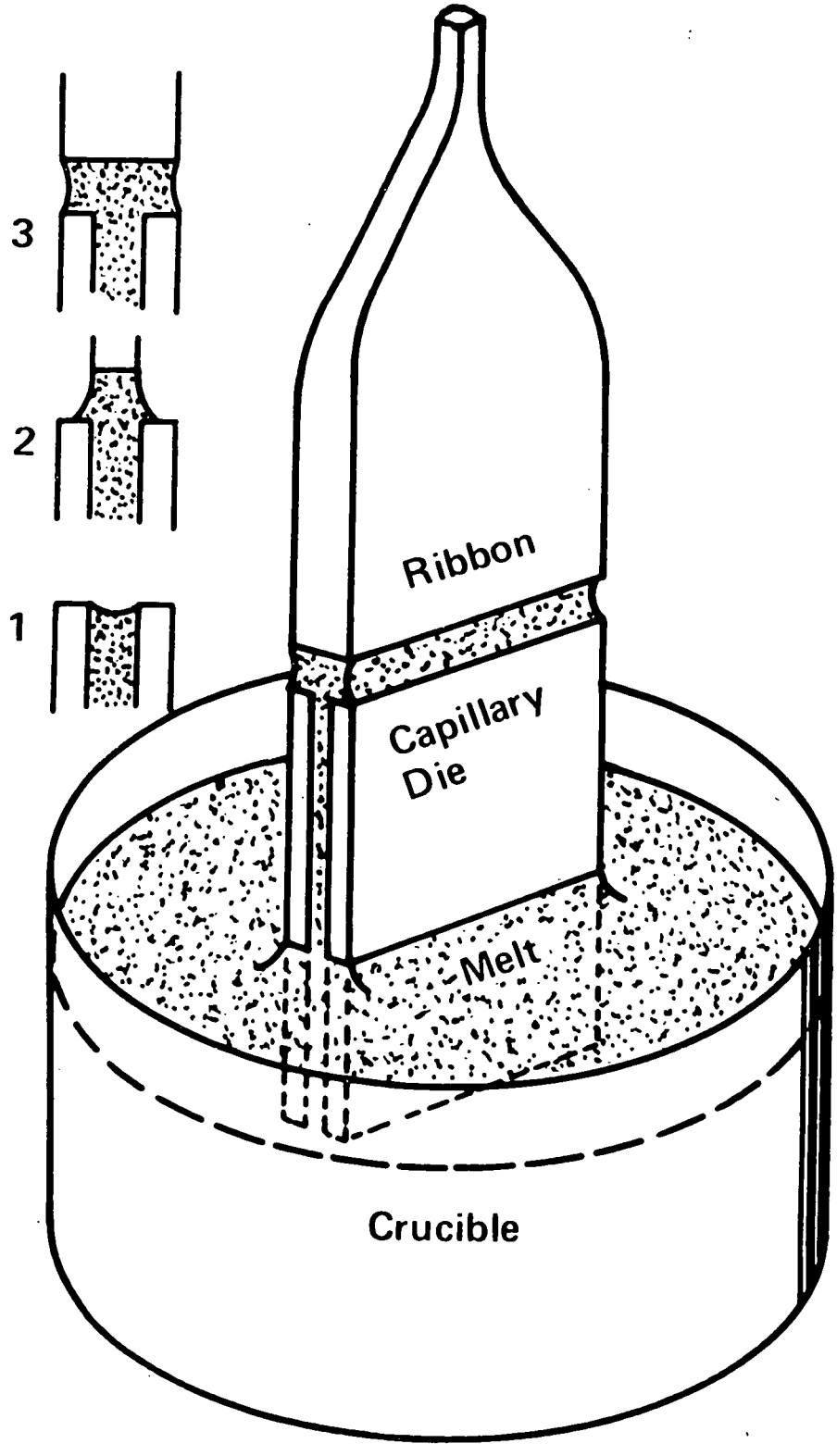

Fig. 1. A schematic diagram of the capillary action shaping technique for silicon ribbon growth.

marred by planar, line, and point defects. Our objective in this work is to attain a clearer technological assessment of silicon ribbon growth by the capillary action shaping technique and to enhance the applicability of the technique to photovoltaic power device material.

The third-quarter progress in crystal growth is presented in three sections: Growth of Silicon Ribbons from Non-Graphite Dies, Effect of Thermal Modifiers on Ribbon Thickness Uniformity and Stress, and Dopant Distribution in Silicon Ribbons.

Ribbons 25 mm in width and up to 0.5 m in length have been grown from SiC dies, and some new characteristics of growth from such dies have been identified. Thermal modifiers have been studied, and systems were developed which reduce the frozen-in stress in silicon ribbons and improve the thickness uniformity of the ribbons. Preliminary spreading-resistance measurements indicate that neither surface striations nor twin boundaries give rise to appreciable resistivity variations, but that large-angle grain boundaries cause local resistivity increases of up to 200%.

2. GROWTH OF SILICON RIBBONS FROM NON-GRAPHITE DIES

Additional manufacturer's data on the hot-pressed die materials reported in the last quarterly report have been

obtained and are shown in Table I.

TABLE I. Manufacturer's Data on Hot-Pressed Die Materials

Material	Particle Mesh Size	Binder	Purity (%)	Typical Theoretical Density (%)
AlB_{12}	325	None	99	90
TiB_2	325	None	99	90
Al_4C_3	325	None	99	90
ZrB_2	325	None	99	90
B_4C	800	None	99.9	90
Si_3N_4	325	None	99.8	65

Purity analysis of ribbons grown from experimental die materials has not yet been completed.

Dies for 25-mm-wide ribbon growth have been fabricated from Carborundum Company KT silicon carbide. Several ribbons 0.5 m long x 25 mm wide were successfully grown from this die material. In each growth attempt, it was observed that liquid silicon entered the region between the die and the die holder. While the cause has not been uniquely determined, we speculate that the die material itself is acting as a wick for the silicon melt. The melt in contact with the graphite die holder may tend to contaminate the remaining

melt with carbon, obscuring the dissolution behavior of the SiC die.

A distinct difference in the morphology of silicon carbide particle formation at the die top was seen between graphite and silicon carbide dies. In the case of graphite dies, individual yellow β-SiC crystals form at the top and on its sides (see Quarterly Technical Progress Report Number 1, August 1975). With the KT silicon carbide dies, a dense, continuous film of SiC tends to grow from the carbon-saturated silicon melt near the die top. When the die is first used, this film does not interfere appreciably with the Si ribbon growth. The initial ribbon perfection (both with KT SiC and with Crystar SiC) can be quite good, as indicated in Fig. 2. As ribbon growth progresses, however, the SiC film also grows and, at some stage, begins to break loose from the die top in clumps, which are then incorporated in the ribbon (Fig. 3) and disturb its perfection. The frequency of this occurrence is similar to that of SiC crystallite incorporation with graphite dies, and the appearance of the grown ribbons is not too different from that of ribbons grown with graphite dies (Fig. 4).

It is felt that further progress may be possible with dies of pure, dense silicon carbide grown by CVD or single-crystal technique, if the wetting between the die and the die holder can be prevented.

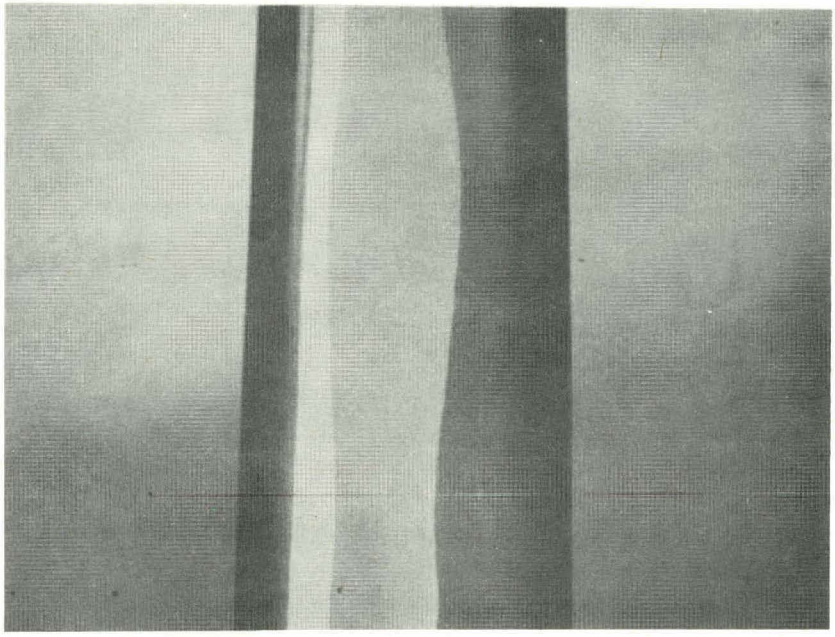

Fig. 2. Ribbon section near seed end, with use of SiC die and (111) face seed. Note facet indicative of good perfection.

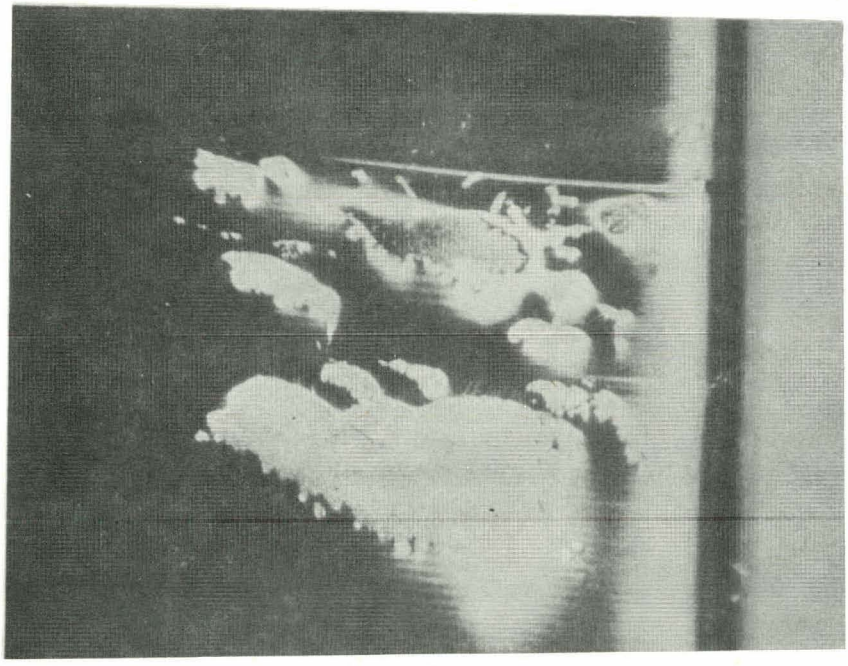

Fig. 3. Clump-like particles embedded in silicon ribbon when KT SiC die is used (60x).

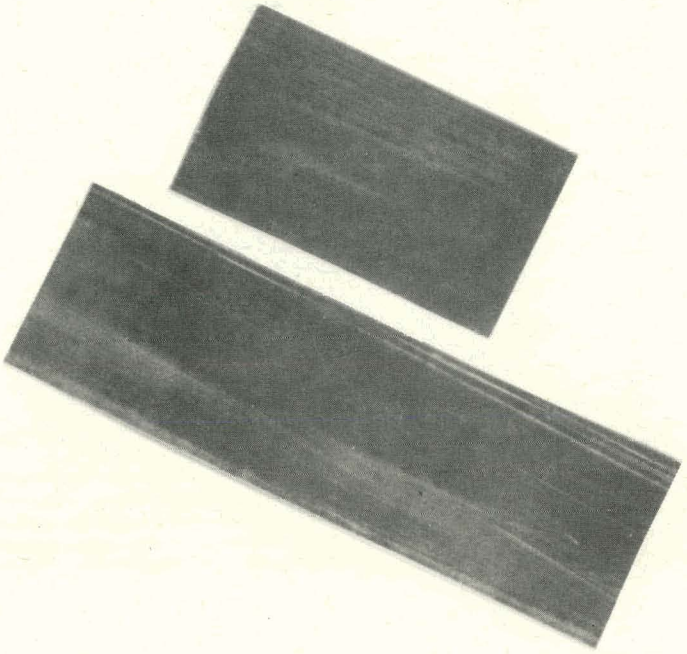

Fig. 4. Appearance of silicon ribbons, 25 mm in width, grown from KT SiC die (bottom) and POCO graphite die (top).

3. EFFECT OF THERMAL MODIFIERS ON RIBBON-THICKNESS UNIFORMITY AND STRESS

Several graphite thermal modifiers have been tested to determine their effect upon two ribbon parameters--transverse thickness uniformity and "frozen-in" stress. The modifiers are passive in that they are not independently variable with respect to the rf susceptor heater. Their design has evolved in an empirical fashion.

The basic setup to which the thermal modifiers have been applied, shown schematically in Fig. 5, consists of the susceptor, die holder, die, lower shield, upper shield,

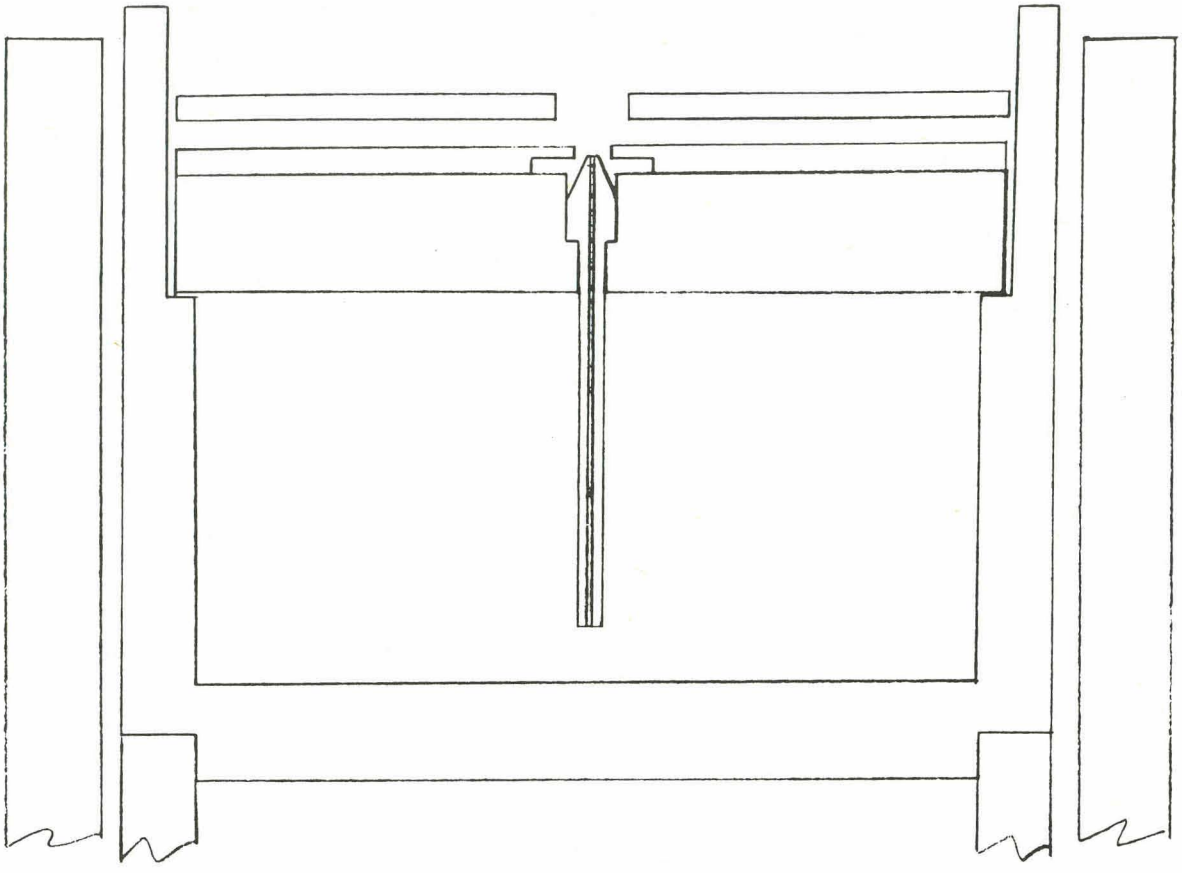

Fig. 5. Cross-sectional view of hot zone in basic setup.

and opaque cylindrical quartz insulator. In the basic setup, the quartz insulator has a 64-mm ID, with a 6-mm wall, and its top is 2 mm lower than the susceptor top. The die top protrudes 1.0 mm above the top plane of the die holder, which is 9.53 mm thick. The susceptor top is recessed 18.3 mm deep to accept the die holder and shields. The upper part of the susceptor wall is 2.67 mm thick, and the lower part is 4.57 mm thick. The susceptor OD is 60.2 mm. The lower shield is 1.57 mm thick. It has a 2.38 mm x 27.78 mm slot, and the bottom is recessed 0.76 mm deep x 7.94 mm wide x 33.34 mm long. A 1.27-mm-thick spacer (not shown in Fig. 5) separates the bottom and top shields. The top shield is 1.27 mm

thick with a 4.76 mm x 30.16 mm slot. The 10-turn rf coil used with the setup is placed so that 2 turns are above the susceptor top and 8 turns are below. The coil has a nominal length of 100 mm and a diameter of 100 mm. The susceptor, shields, and die holder are made of graphite.

The first thermal modifier tried was a 50-mm-ID graphite tube, 67 mm high, with a 5-mm wall thickness. This tube rested on the top rim of the susceptor and had a 12.7-mm-diameter viewing port drilled through the wall. Five growth attempts were made with the tube in place. In all attempts, freezing of the liquid film between the die and the ribbon occurred before the ribbon had spread from seed width (4 mm) to full width.

The second modifier system consisted of a molybdenum plate 53.6 mm in diameter and 1.59 mm in thickness with a central slot 4.76 x 30.16 mm. Vertical parallel plates projected upward along the sides of the slot. These were 12.7 mm high x 22 mm wide x 1.59 mm thick and separated by a distance of 4.76 mm. The modifier rested on the upper heat shield. Five growth attempts indicated that this system was also prone to premature freeze-out. In addition, a short full-width ribbon grown with this modifier was very non-uniform in thickness, with the edges being thicker than the middle.

The third modifier was a 12.7 mm thick x 53.6 mm diameter graphite block which rested on the upper shield. The opening through which the ribbon was pulled was tapered from a 7.1-mm width at the bottom surface to an 18.5-mm width at the top surface. Ribbon growth was easier with this setup, and five full-width ribbons were grown at speeds ranging from 14 to 23 mm/min. The average ratio of edge thickness to center thickness at the tail end of the ribbons was 1.59 and did not correlate with growth speed. Actual thickness tended to decrease with increasing growth speed for a given die (e.g., at 14 mm/min, the maximum and minimum thicknesses were 0.51 mm and 0.36 mm; at 20 mm/min, the corresponding values were 0.41 mm and 0.25 mm). The ribbon surface appeared to be duller with this modifier than without it, potentially indicating a thicker SiC vapor-grown film on the ribbon. Ribbon 51104, grown at 14 mm/min with the modifier, was deliberately split at the tail end. The split width vs distance curve is shown in Fig. 6.

The fourth thermal modifier system was identical with the third except that the opaque quartz insulator was 15 mm taller. In this case, it was observed that the reduction in system temperature required to proceed from seed width to full-ribbon width was only 30% of that used without a thermal modifier. Growth was susceptible to freeze-out unless carried out slowly. The tail-end, edge/middle

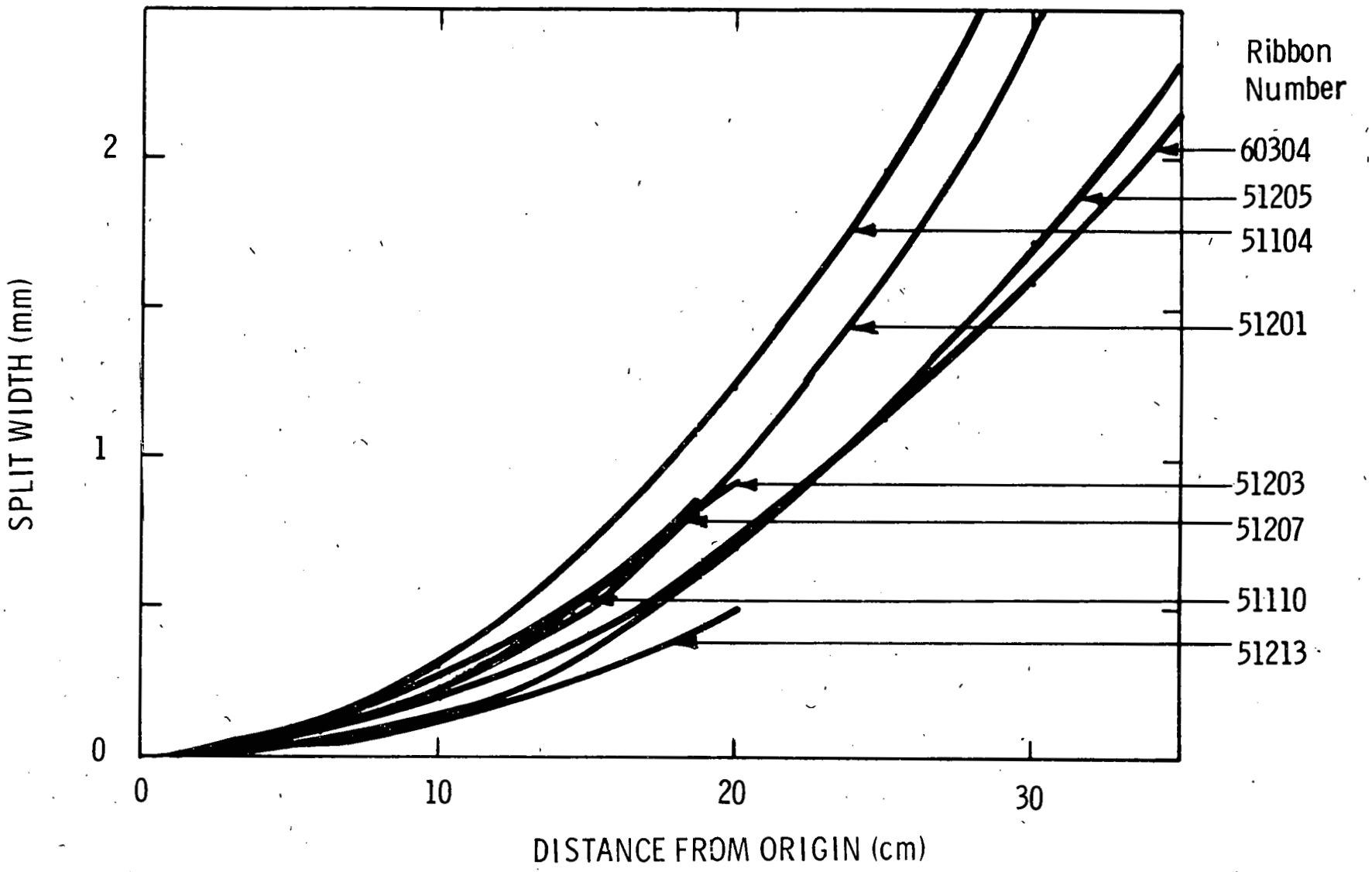

Fig. 6. Split width vs distance from split origin for deliberately split ribbons.

thickness ratio of a ribbon grown at 11 mm/min was only 1.10, and the middle thickness was 0.50 mm. The thickness ratio increased to 1.43 at 18 mm/min, and the middle thickness correspondingly decreased to 0.35 mm. Stress levels of ribbons grown at 11 mm/min (No. 51110), 12 mm/min (No. 51203), and 18 mm/min (No. 51202) with this modifier were lower than that seen with the third modifier system.

The fifth thermal modifier to be tried consisted of two graphite blocks with recessed vertical grooves (see Fig. 7), which were placed at the edges of the ribbon. The blocks

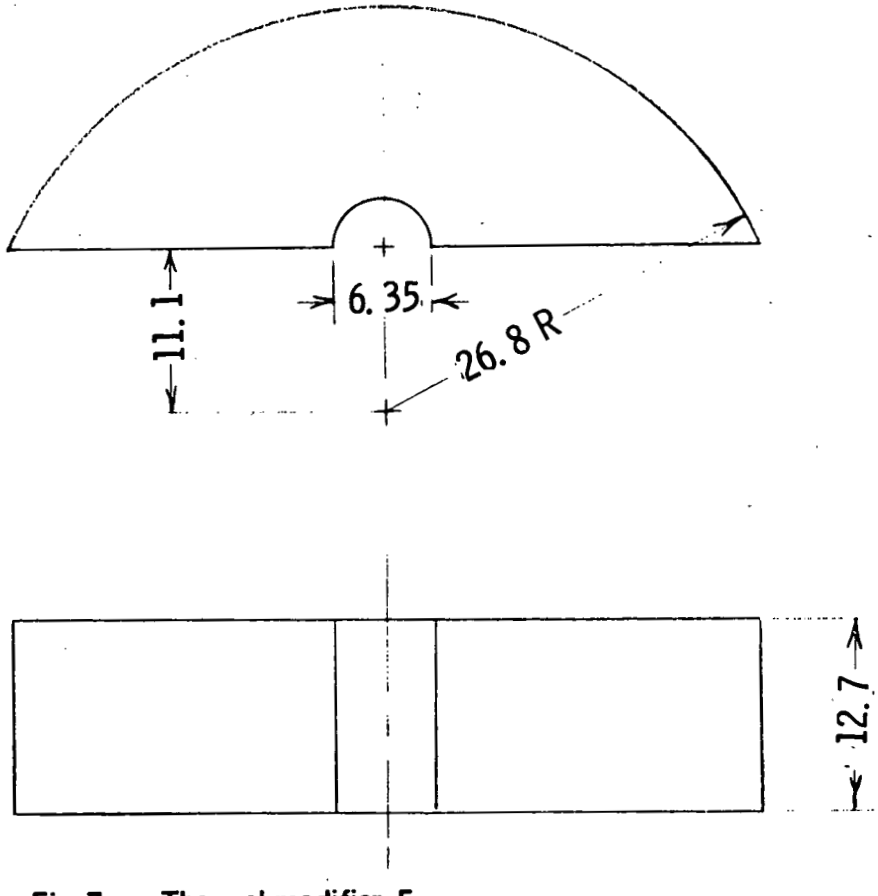

Fig. 7. Thermal modifier 5.

rested on the upper heat shield. Three full-width ribbons were grown with this modifier. The average edge/middle thickness ratio at the tail ends was 1.19 for growth rates of 17-19 mm/min. Even though the growth rates did not vary appreciably and the same die was used, quite a difference in average thickness was seen among the ribbons. Ribbon 51207 was 0.24 mm thick and had a stress level comparable to that seen with modifier No. 4. Ribbon 41205 was 0.47 mm thick and had a lower stress level (see Fig. 6).

The sixth thermal modifier system was like the fifth, except that the quartz insulator was 15 mm higher than in the basic setup. Three ribbons were grown, and it was found that approximately uniform ribbon thicknesses could be produced at selected growth rates. Ribbon 51210 was grown at 14 mm/min and exhibited an inverted thickness profile; the edge-to-middle thickness ratio was 0.77. The edge thickness was 0.50 mm, and the middle thickness was 0.65 mm. Three attempts were made to split this ribbon deliberately, and, in each case, the crack veered to the ribbon edge instead of propagating up the ribbon. Thus the frozen-in stress was very low. As the speed was increased to 18 mm/min (ribbon 51213), it was possible to split the ribbon, but the stress level was still relatively low (see Fig. 6). At this speed, and at 17 mm/min (ribbon

51214), the ribbon did not exhibit an edge/middle thickness variation; the ribbon cross section was slightly wedge-shaped, with one edge 0.45 mm thick and the other 0.41 mm thick. This probably reflects non-uniform machining of the die.

In the seventh thermal modifier system, an attempt was made to combine the uniform-thickness capability of system number six with a still lower stress level. Towards this end, a modifier was assembled in modular form, as follows. System number six was first assembled. On top of the 12.7-mm blocks, spacer blocks 20 mm high x 37 mm wide x 10 mm thick were placed so that the flat 20 mm x 37 mm surfaces were near and perpendicular to the edges of the ribbon. On top of the spacer blocks was placed a graphite cylinder 53.6 mm in diameter x 12.7 mm high. The latter had a 6 mm x 40 mm milled slot through which the ribbon was withdrawn, as well as a cutout at its edge for viewing purposes. It was hoped that the block would reduce the vertical thermal gradient to some extent and in this way reduce the frozen-in stress. Ribbon 60105 was grown at a speed of 14 mm/min and was found to resist splitting (Fig. 8). The ribbon was essentially uniform in thickness, with a slightly wedge-shaped cross section (0.50 mm thick at one edge and 0.45 mm thick at the other).

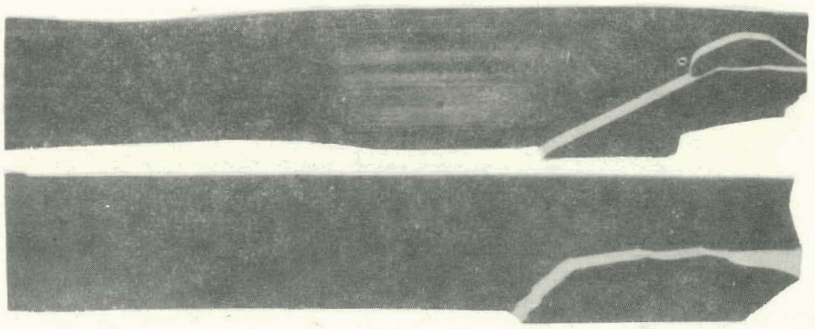

Fig. 8. Two 25-mm-wide ribbons which resisted attempts at axial splitting. Top, ribbon 60203; bottom, ribbon 60105.

In thermal modifier number 8 (see Fig. 9), an attempt was made to incorporate and enhance the main features of modifier number 7 in a one-piece design. Several ribbons were grown with this modifier, and, indeed, good resistance to splitting was seen (see Fig. 8, ribbon 60203). However, a very high edge/middle thickness ratio was obtained. Ribbon 60202, for example, was grown at 18 mm/min and had an edge/middle-thickness ratio of 1.57. The central thickness was 0.30 mm.

For comparison purposes, ribbon 60304 was grown at 20 mm/min, using the basic setup with no additional thermal modifiers. The observed splitting (Fig. 6) was comparable to that seen with ribbon 51205, which was grown using the fifth thermal modifier system. However, the edge-to-middle thickness ratio was 1.91--much higher than was observed with modifier number 5. The middle thickness was 0.22 mm.

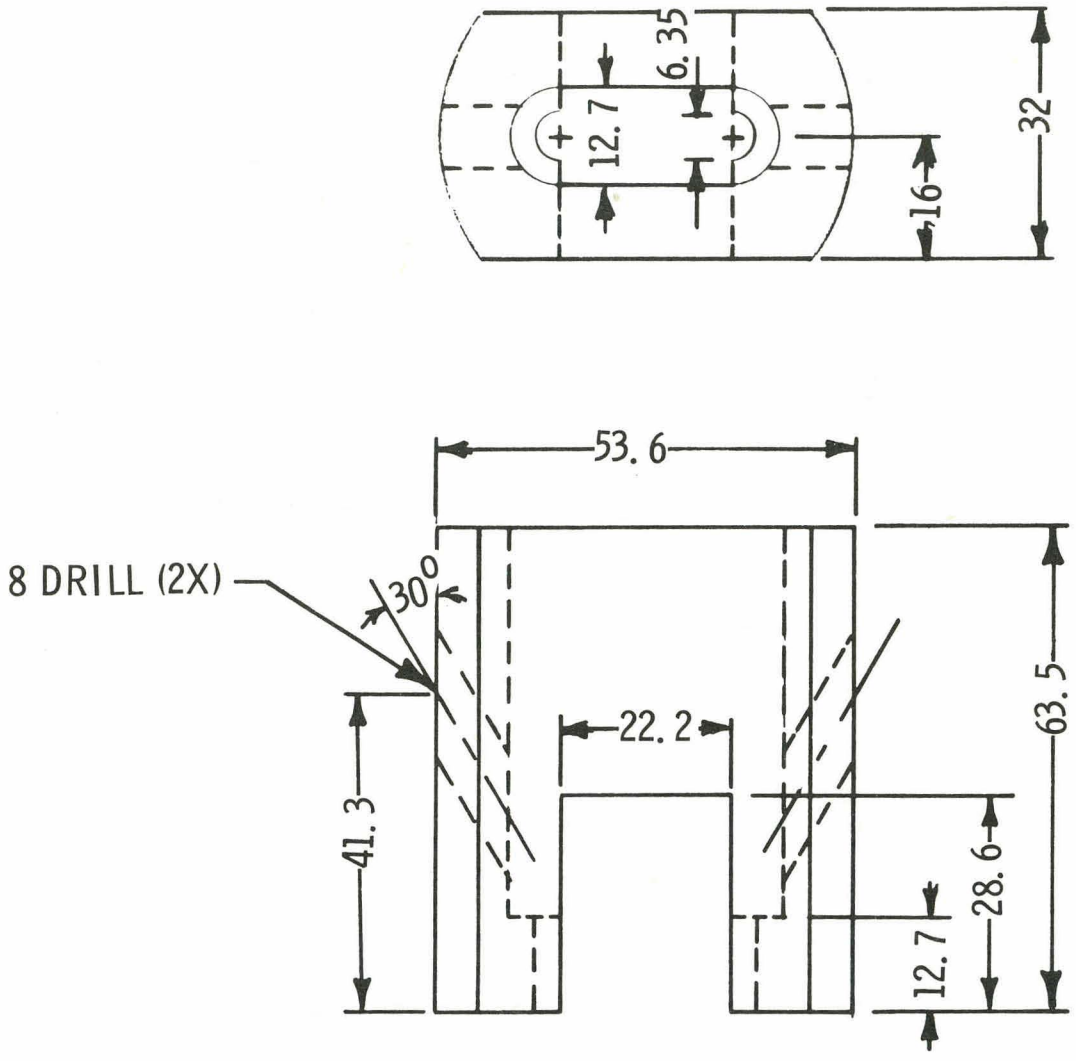

Fig. 9. Thermal modifier 8.

Although the parameters involved are numerous, the observed behavior of passive thermal modifiers can be essentially summarized as follows:

1. Placing relatively massive graphite thermal modifiers, preferentially, near the edges of the ribbon tends to reduce the edge thickness relative to the middle thickness and, at an optimum growth speed, results in approximately uniform

ribbon thickness (e.g., the sixth thermal modifier system, at 17-mm/min growth speed).

2. Decreasing the vertical thermal gradient by extending the height of the thermal insulation or by adding massive, passive graphite thermal modifiers around the ribbon at some distance above the growth interface tends to reduce or eliminate the tendency for splitting to propagate along the ribbon (e.g., the seventh and eighth thermal modifier systems).

As determined from uncorrected optical pyrometer measurements on "interior surfaces" of the graphite components in the basic setup, with thermal modifier number 8 in place, the temperature profile of Fig. 10 is present in the proximity of the ribbon edges during growth and is sufficient to produce non-splitting ribbons, such as 60203.

4. DOPANT DISTRIBUTION IN SILICON RIBBONS

In the second quarterly progress report, a non-uniform transverse doping profile was presented for the 25-mm-wide boron-doped silicon ribbons, via spreading resistance measurements. The resistivity within 3 mm of the ribbon edges and in the central 5 mm of the ribbon was observed to be only about 20% of the value at other positions along the width of the ribbon. In the meantime, we have investigated other potential sources of dopant-distribution anomalies.

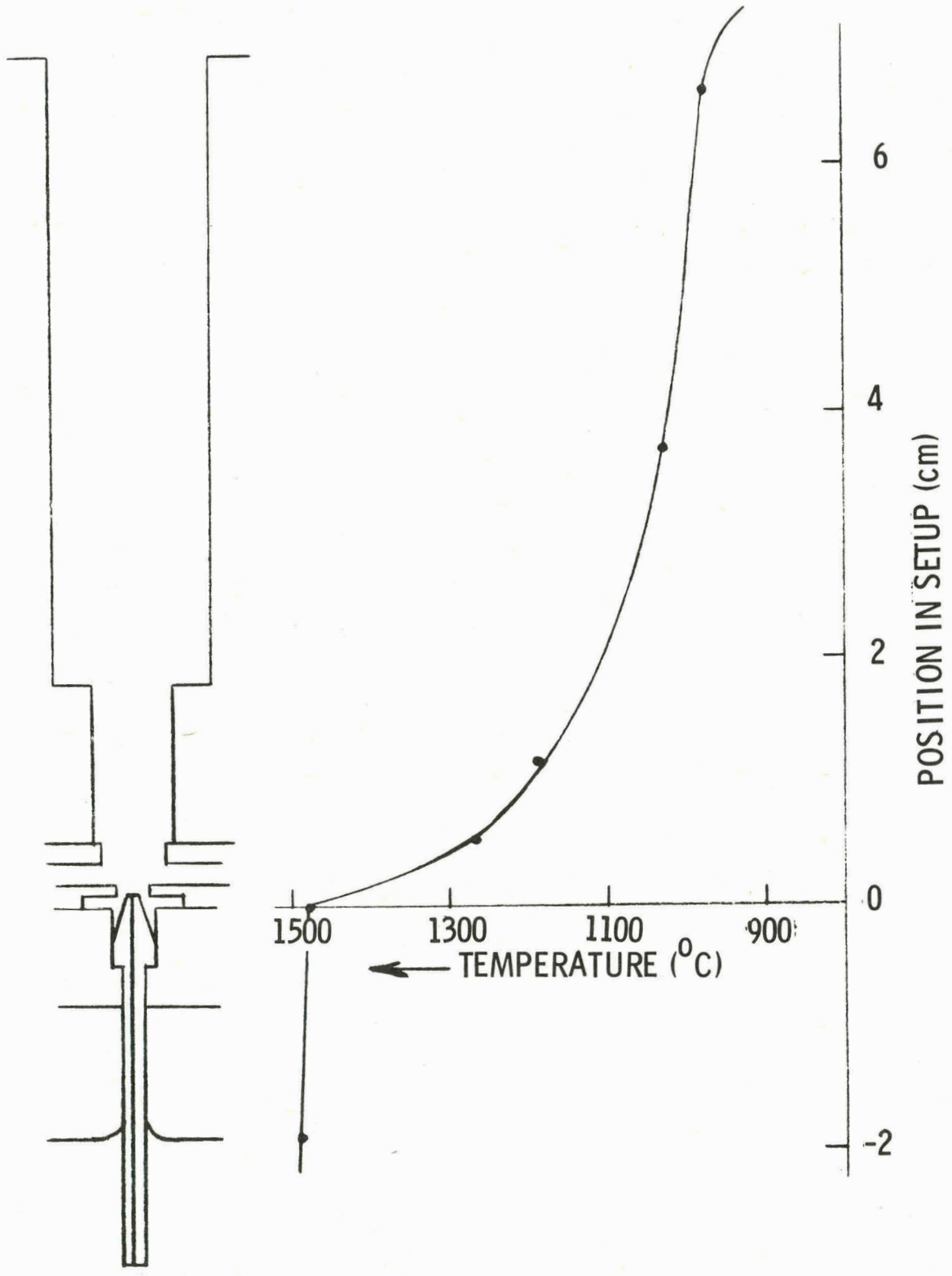

Fig. 10. Thermal profile near edge of ribbon sufficient for low stress levels.

To determine whether or not the surface striations which are incorporated in our ribbons at a frequency of about 30/sec correlate with dopant-distribution striations, we beveled a ribbon at a 3.5° angle (top, Fig. 11) so that spreading-resistance measurements could be made at 2.5-μm intervals, on the lapped surface, in a direction perpendicular to the striation lines. The striation lines, in this case, were spaced at approximately 10-μm intervals and had a nearly sinusoidal peak-to-valley undulation with an amplitude of about 0.37 μm (as calculated from the bevel angle and the structure at the bevel/surface intersection in Fig. 11). Resistance fluctuations of up to about 12% are evident, but do not appear to correlate with the surface striations.

Spreading-resistance measurements were also made on a lapped ribbon surface in a direction perpendicular to a series of twin lines. The surface was then lightly etched to delineate the twins and the probe marks. No appreciable resistance fluctuations were seen in crossing the twin lines (Fig. 12). In another ribbon sample, the resistance was measured across large-angle grain boundaries. The lapped sample was again lightly etched and, in this case, a large increase in spreading resistance (about 200%) was seen upon crossing the grain boundaries, although the resistance in off-boundary regions was reasonably constant (Fig. 13). Thus, the boundaries either tend to exclude the boron dopant or are contaminated with N-type impurities.

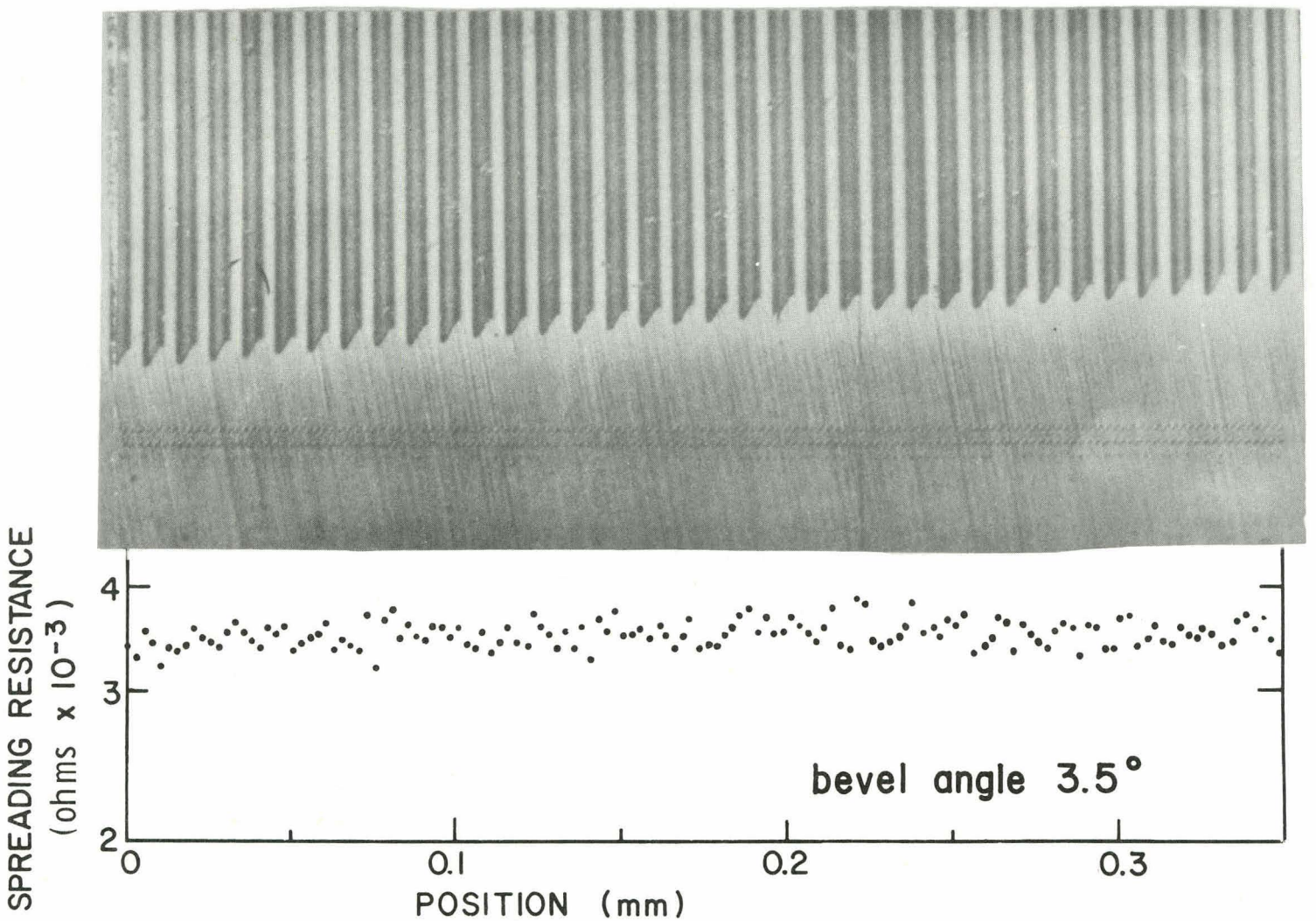

Fig. 11. Spreading-resistance measurements, on a 3.5° beveled surface, perpendicular to surface striations.

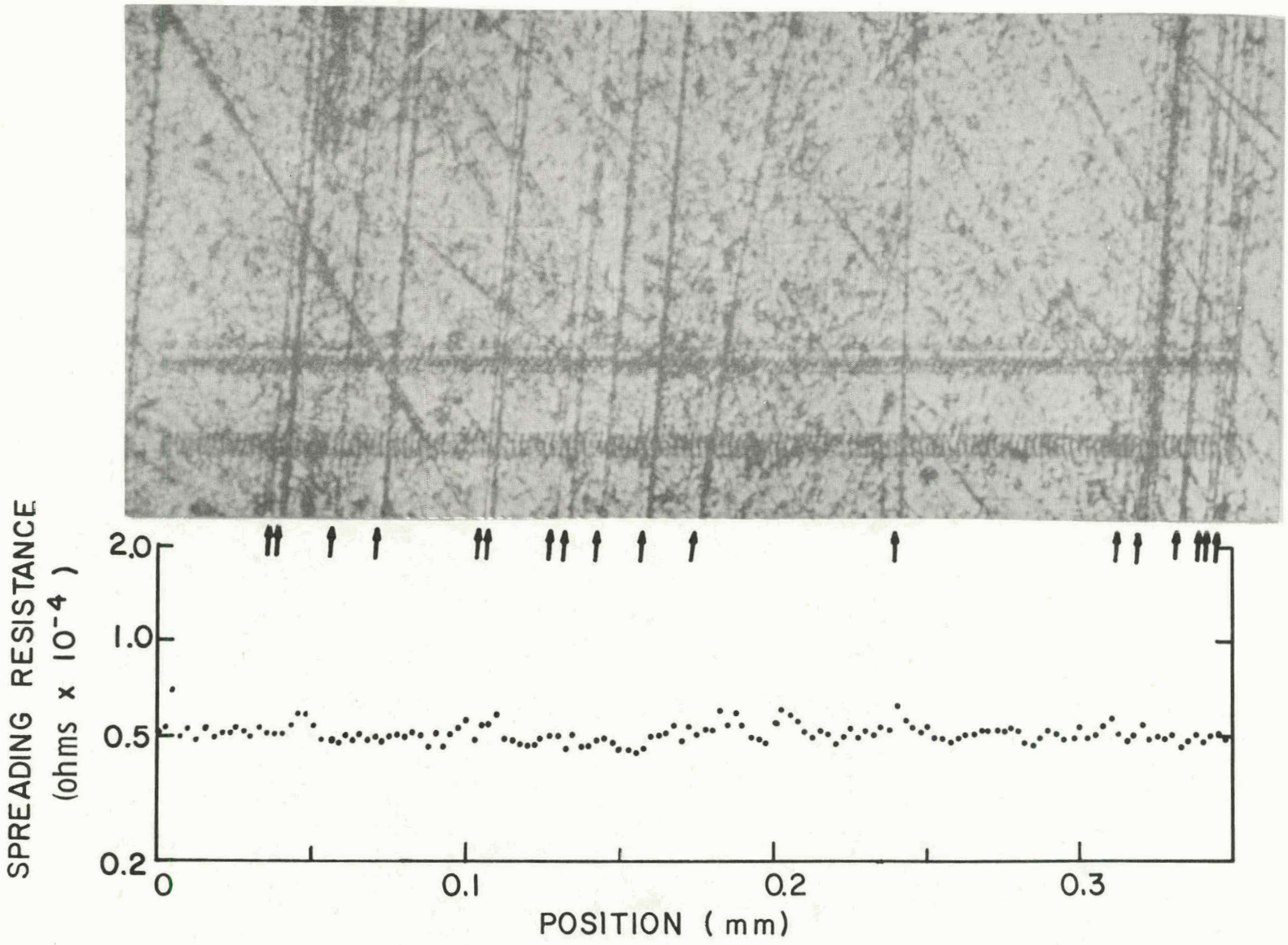

Fig. 12. Spreading-resistance measurements across twin boundaries.

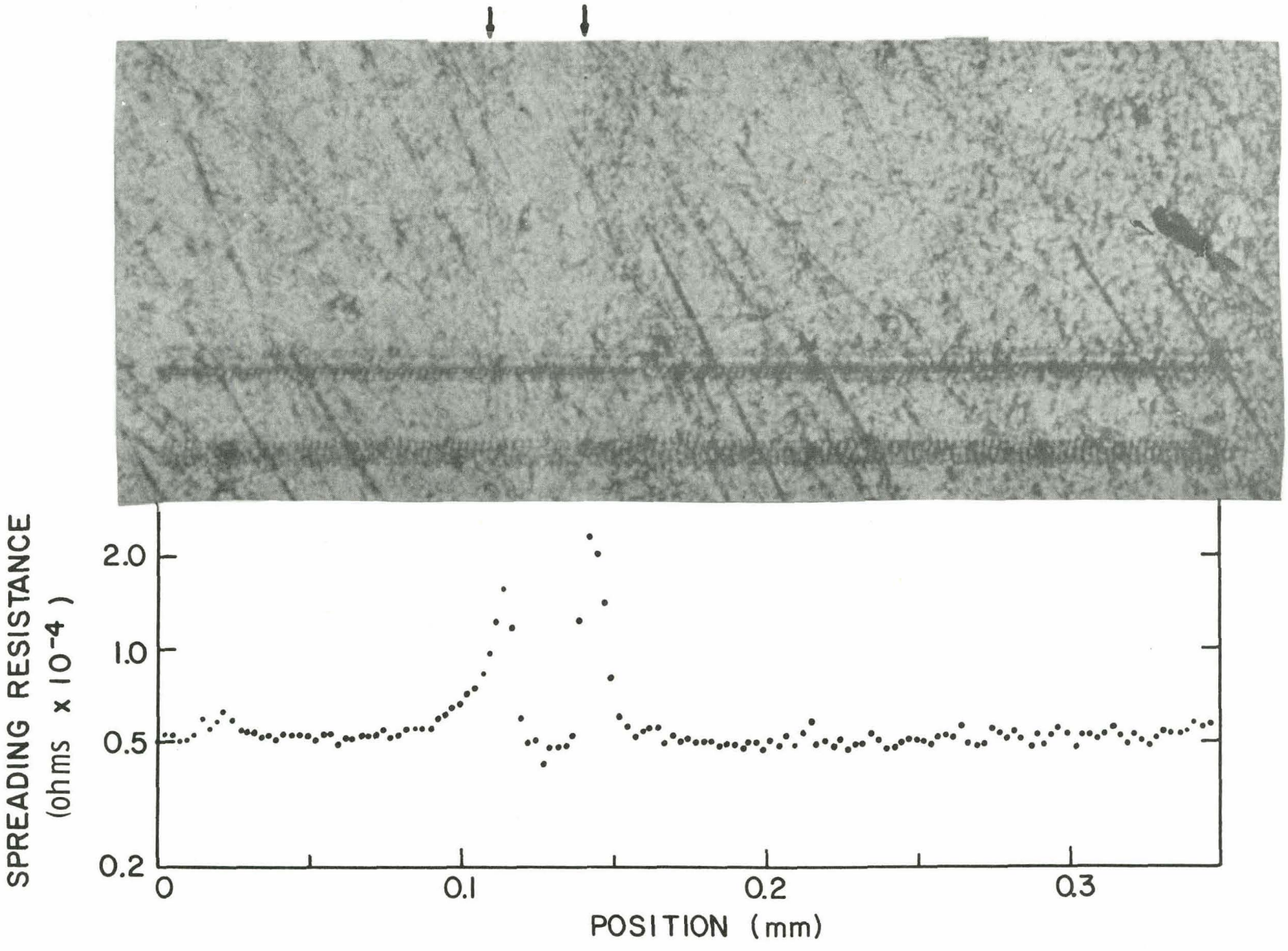

Fig. 13. Spreading-resistance measurements across grain boundaries.

It appears that grain boundaries and the so-far-unexplained transverse dopant-distribution anomaly are our known sources of large-scale resistivity fluctuations while twin boundaries and surface striations have a minor, and perhaps negligible, effect upon resistivity.

5. REFERENCES

1. H. E. LaBelle, Jr., Mater. Res. Bull. 6, 581 (1971).
2. T. F. Ciszek, Mater. Res. Bull. 7, 731 (1972).
3. T. F. Ciszek and G. H. Schwuttke, Phys. Status Solidi (a) 27, 231 (1975).
4. J. C. Swartz, T. Surek, and B. Chalmers, J. Electron. Mater. 4, 255 (]975).

6. ACKNOWLEDGMENTS

Technical support in crystal growing was provided by F. Newman. Spreading-resistance measurements were conducted by E. F. Gorey.

CHARACTERIZATION OF RIBBONS

by

G. H. Schwuttke, H. Kappert, R. Dessauer, and K. Yang

1. INTRODUCTION

This report provides further insight into the crystallographic nature of planar defects in ribbons grown by the capillary action shaping technique. Planar defects, such as twin and grain boundaries, are analyzed through the technique of electron channeling patterns (ECPs).

2. ELECTRON CHANNELING PATTERNS

Electron channeling effects in scanning electron microscopy (SEM) studies are of practical interest for several reasons:

- Crystals can be oriented crystallographically while under SEM observation.
- Surface perfection can be judged from the sharpness of the high-order lines in the patterns.
- Interplanar lattice spacings can be obtained, helping in the identification of unknown crystals.

The SEM channeling patterns are useful because they can be generated from areas smaller than 10 μm in diameter by use of the phenomenon of selected area channeling (SAC). The SAC patterns (SACPs) are due to an angular dependence of electron diffraction and absorption. Hirsch and Humphries have discussed basic features of contrast in SACPs based on anomalous absorption effects in the dynamical theory of electron diffraction (1).

The SACP of a crystalline surface is obtained by holding the electron beam at a selected spot on the sample surface while the incident angle of the beam is rocked through a large solid angle. This leads to the formation of pronounced bands and lines at the Bragg angles of the specimen. Electron channeling patterns look very much like Kikuchi patterns and are indexed by analogous methods. Examples of ECPs obtained on single-crystal silicon are shown in Fig. 1.

Although very useful for crystallite orientation studies, ECPs have not yet found wide application. This is due to difficulties in their interpretation encountered in analyzing ECPs, as seen in the SEM, if the crystal orientation does not coincide with a major low-index orientation. Our work is based on the use of computer-generated ECPs which are completely indexed and thus eliminate this problem.

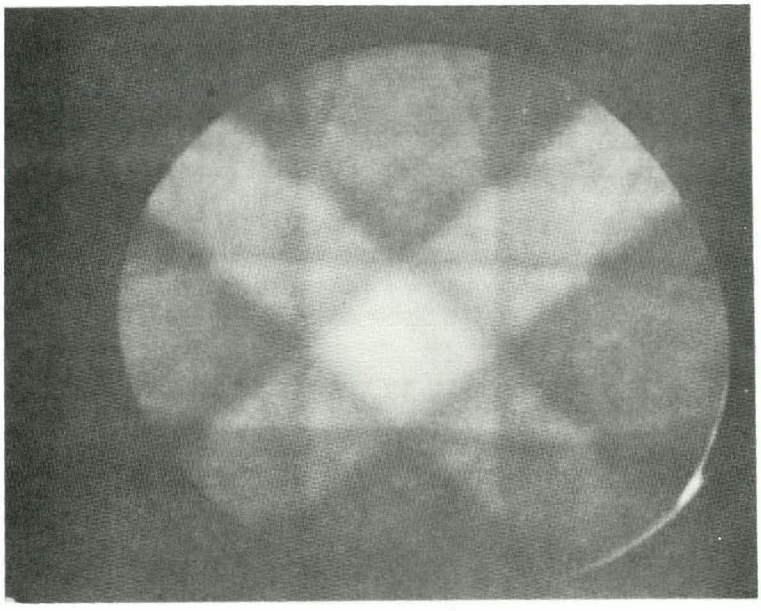

a

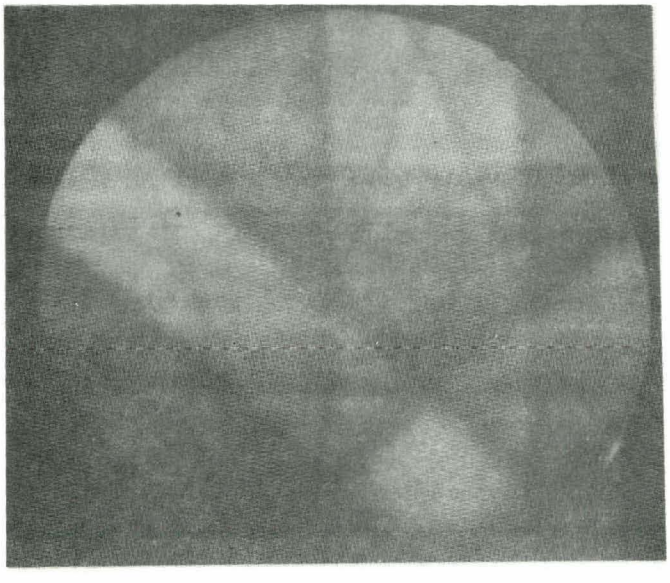

b

Fig. 1. ECP for (001) Si, 30 keV:
(a) 0^{o} tilt and (b) 5^{o} tilt.

2.1 Computer Generation of Indexed ECP Maps

Electron channeling patterns were generated by use of a program previously written to plot Kikuchi patterns for transmission electron microscopy. The patterns are plotted for an energy of 30 keV. Maps are obtained for (001), (011), and (111) poles in the center of the projection. In the generation of the ECPs, the following considerations are used:

- Ribbon analysis requires ECP maps covering 25 degrees around the three main poles. Consequently, ECP lines up to the fourth order and up to $h^2 + k^2 + l^2 = 81$ are plotted. These maps are given in Figs. 2a, 2b, and 2c.

- Ribbon analysis makes it desirable to have an overview of ± 60 degrees around the center pole. Therefore, the center poles are plotted with ECP lines up to the fourth order and $h^2 + k^2 + l^2 = 49$. These patterns are given in Figs. 3a through 3d.

The complete program for the generation of such maps is described in Ref. 2.

3. RIBBON SURFACE ORIENTATION ANALYSIS

Electron channeling patterns are used to determine surface orientations present in ribbons. Four major crystal orientations

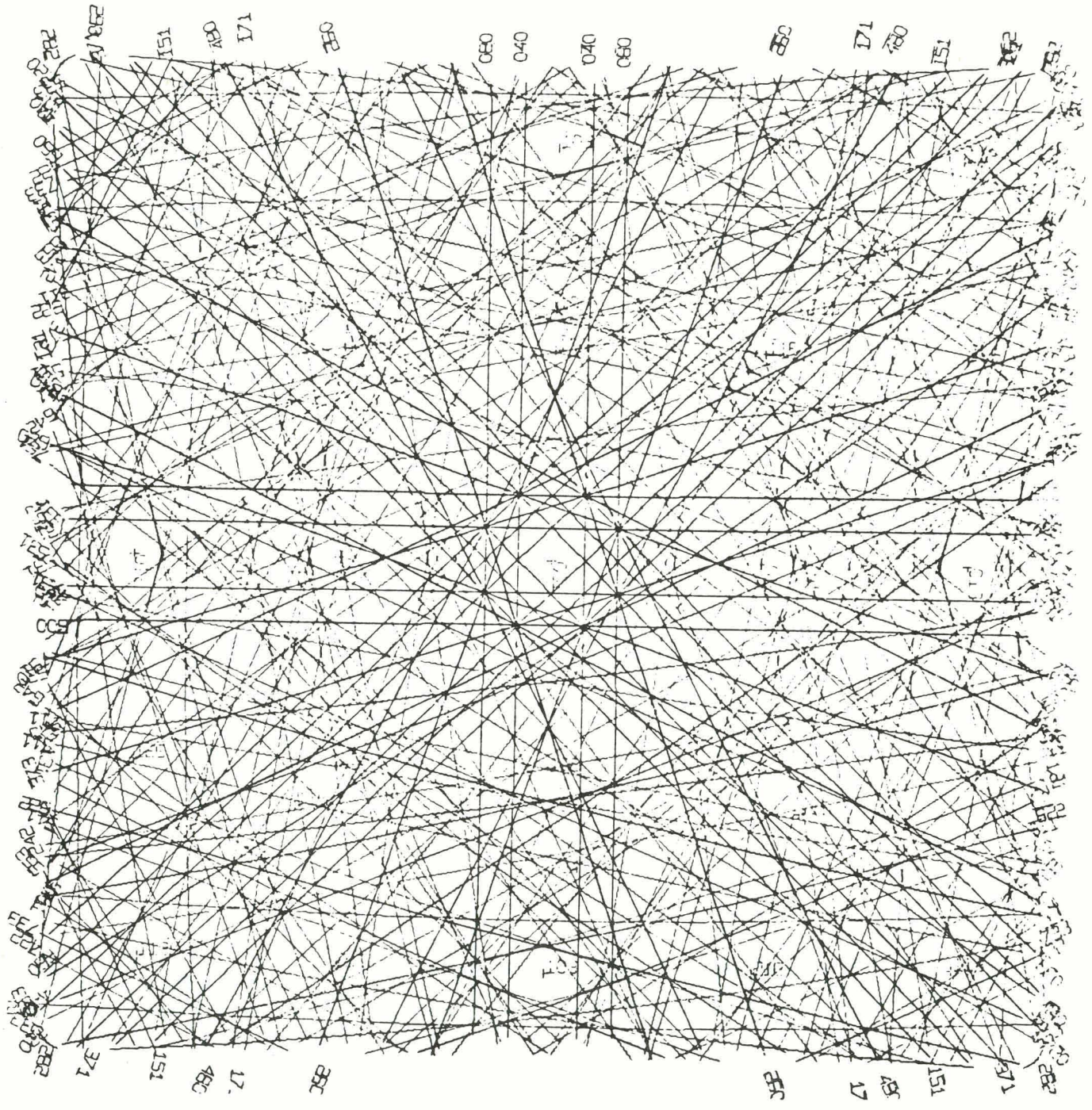

Fig. 2a. ECP map for (001) Si, 30 keV, $x_o = y_o = 12$, R = 32, RMN = 4, and SMSQ = 9.

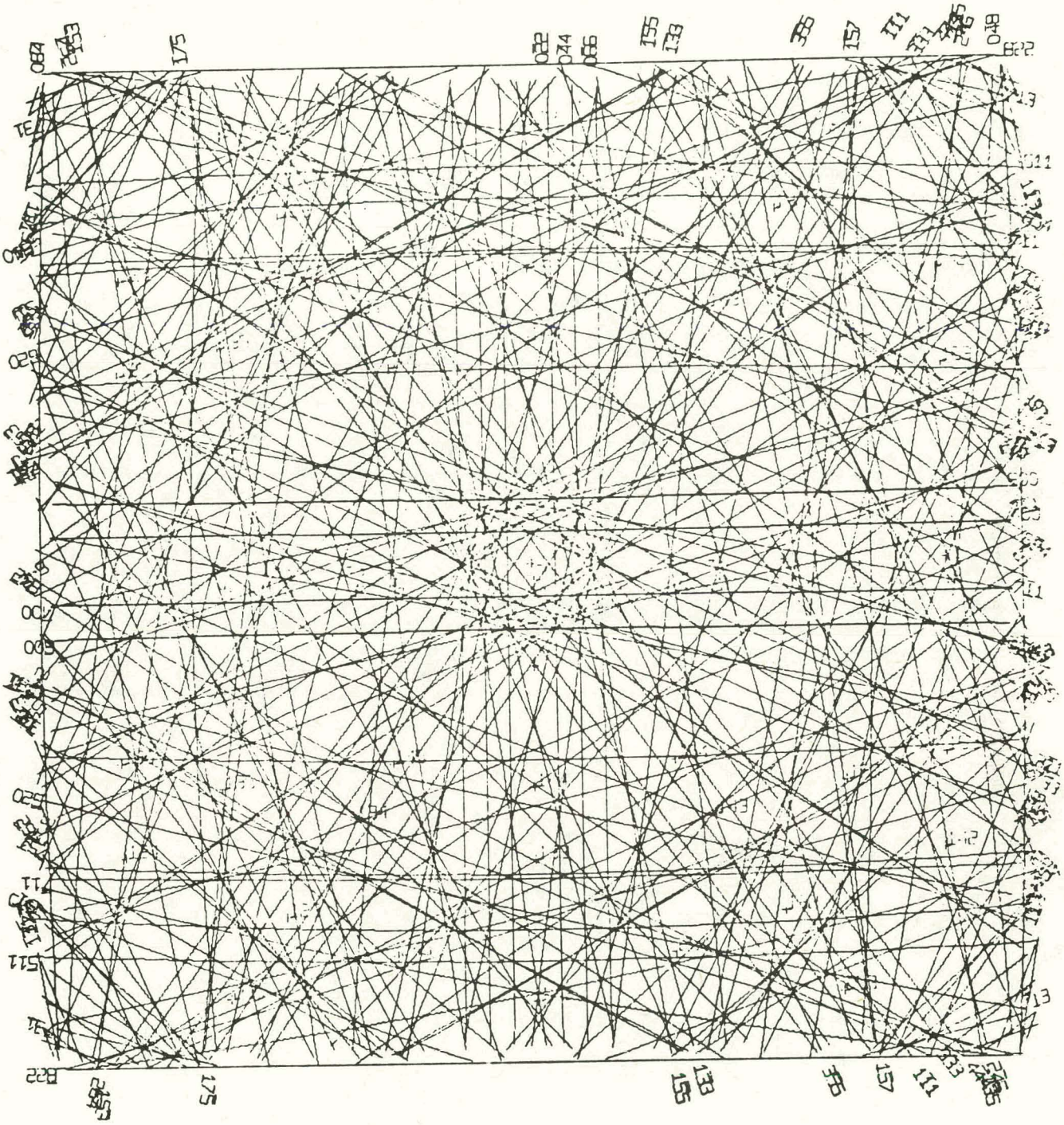

Fig. 2b. ECP map for (011) Si, 30 keV, $x_0 = y_0 = 12$, R = 32, RMN = 4, and SMSQ = 9.

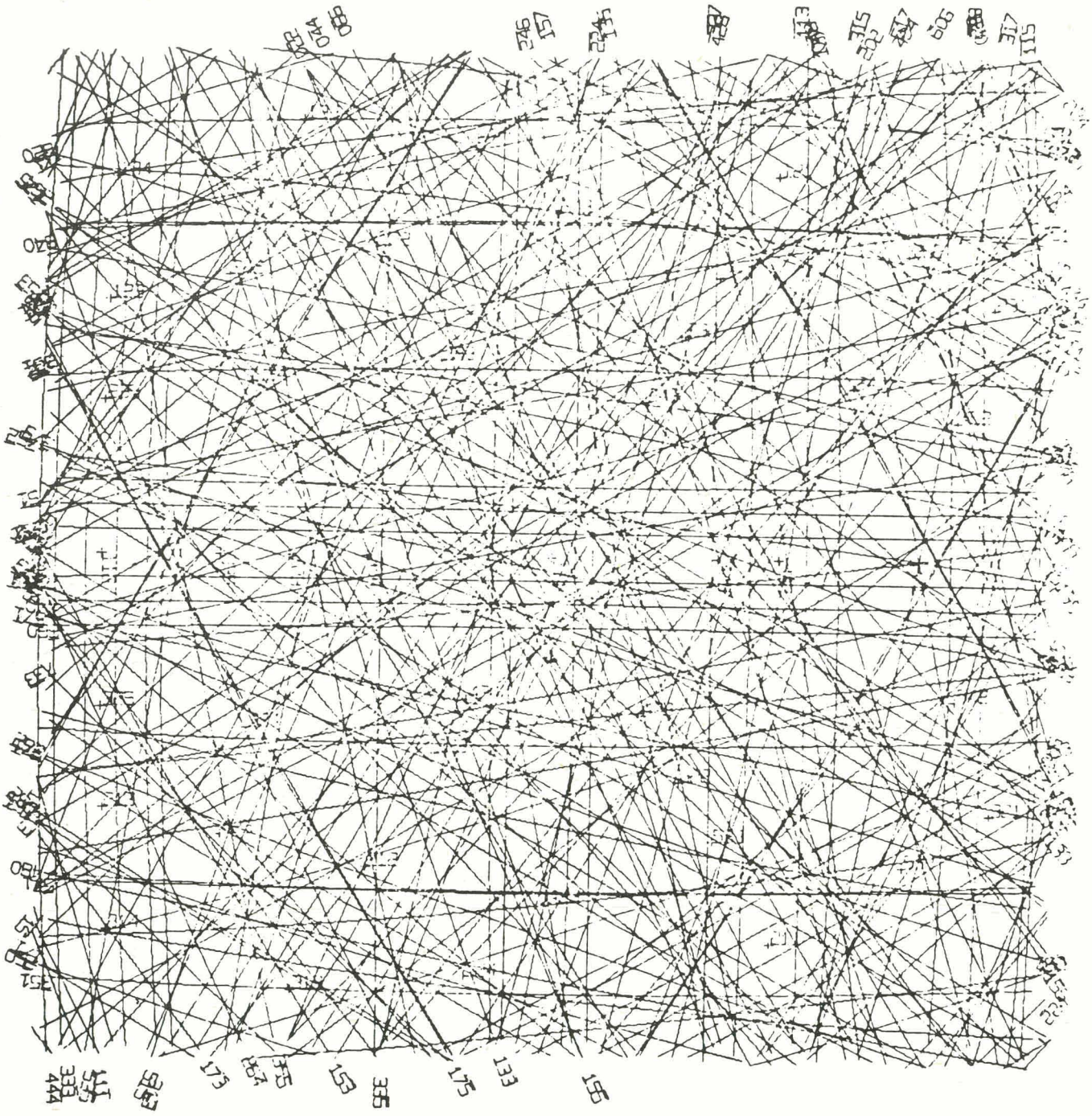

Fig. 2c. ECP map for (111) Si, 30 keV, $x_o = y_o = 12$, R = 32, RMN = 4, and SMSQ = 9.

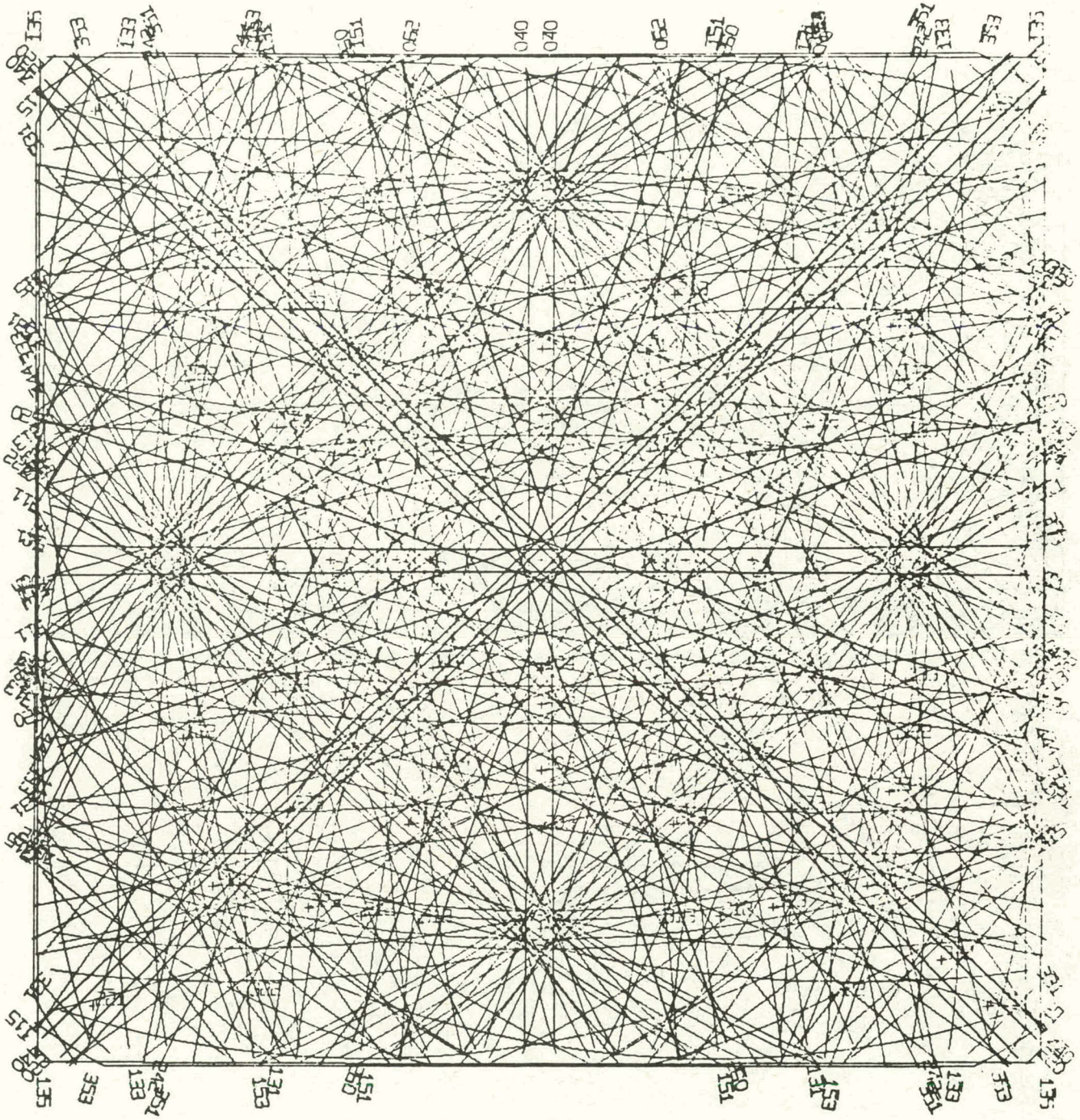

Fig. 3a. ECP map for (001) Si, 30 keV, $x_o = y_o = 12$, R = 11, RMN = 4, and SMSQ = 7.

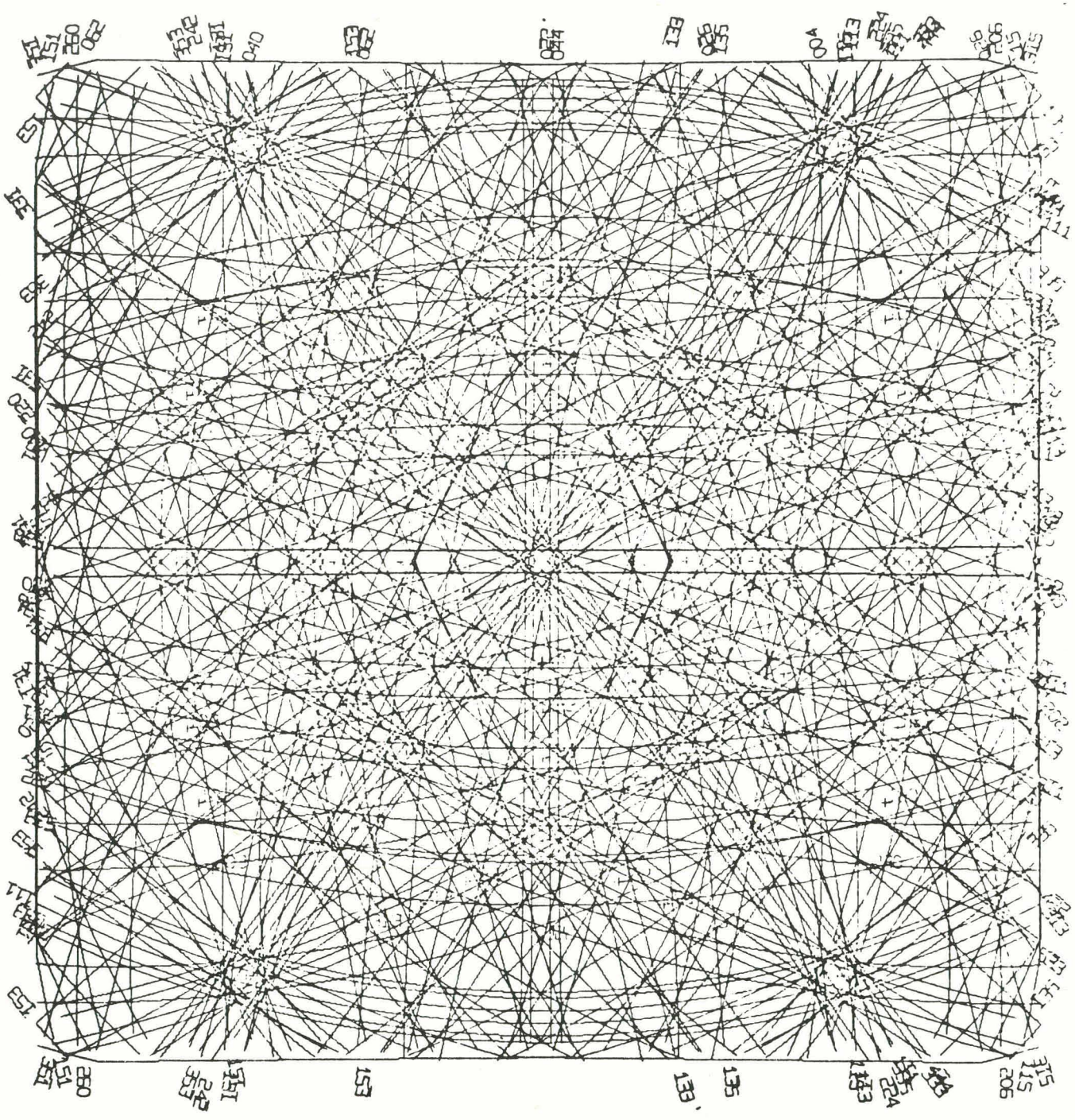

Fig. 3b. ECP map for (011) Si, 30 keV, $x_o = y_o = 12$, R = 11, RMN = 4, and SMSΩ= 7.

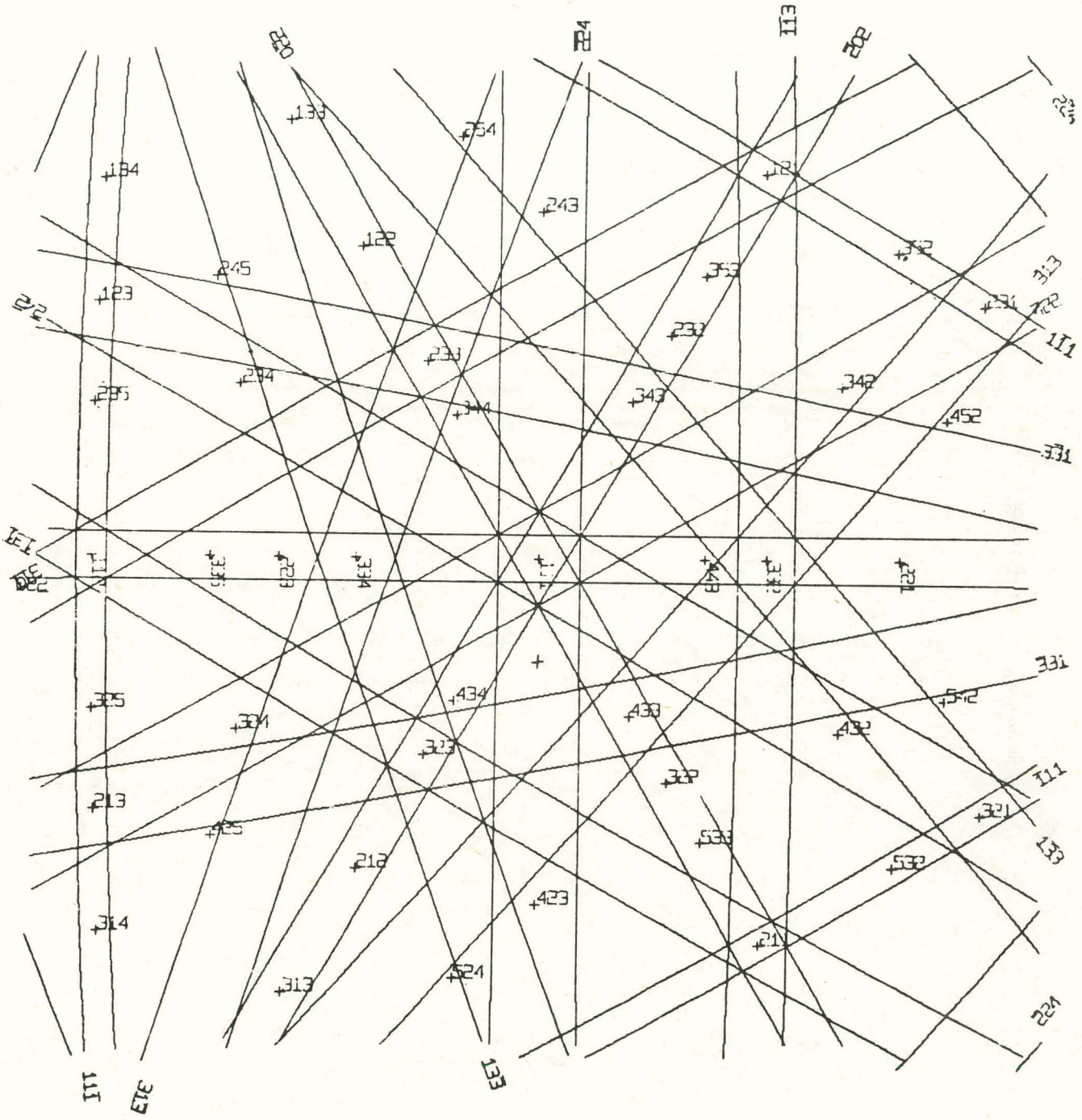

Fig. 3c. ECP map for (111) Si 30 keV, $x_o = y_o = 12$, R = 32, RMN = 1, and SMSQ = 5.

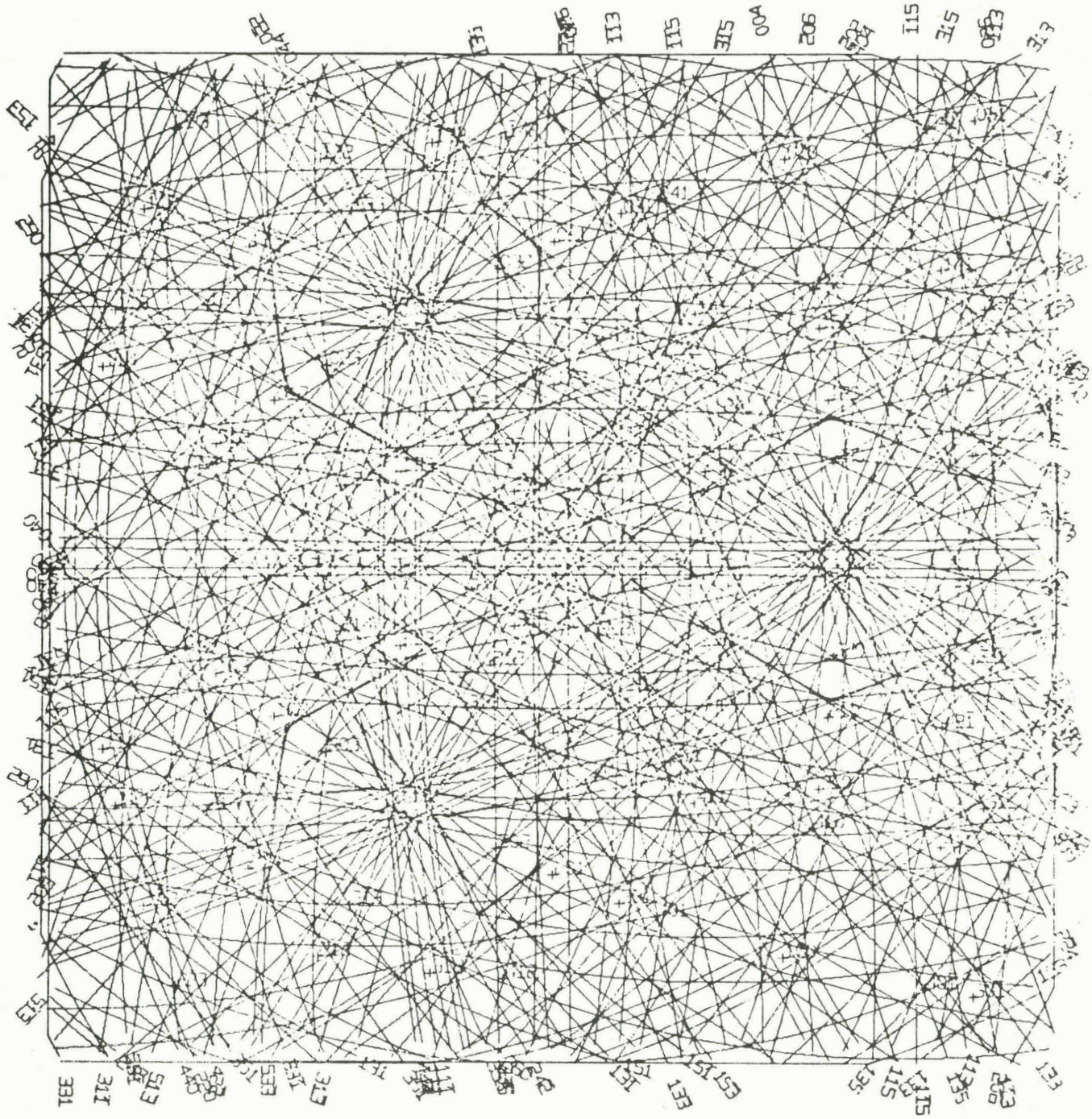

Fig. 3d. ECP map for (111) Si, 30 keV, $x_o = y_o = 12$, R = 11, RMN = 4, and SMSQ = 7.

are identified in ribbons grown with carbon dies: <110>, <111>, <114>, and <115>. Ribbon surfaces may display such orientations independent of the original seed orientation; however, the respective surfaces are misoriented. Misorientation covers a range from 6 to 15 degrees. Two basic twin mechanisms are operative during ribbon growths using carbon dies. The first mechanism leads to repetitive twinning, with twin lines spaced parallel to each in the growth direction. The second twin mechanism leads to nonparallel twin lines and grain boundaries. It is tied to the occurrence of silicon carbide particles in the ribbon surface and can be substantially minimized.

Examples of typical twinning in ribbons grown with a carbon die are shown in the photomicrographs of Fig. 4. Changes in surface orientation of ribbons due to such defects are discussed in the following section.

3.1 Orientation Analysis Through ECPs

The photomicrograph of Fig. 5 shows a ribbon section selected for its complexity of different surface features and is not representative of the IBM state-of-art of ribbon crystal growing. The sample of Fig. 5 is useful for demonstration of the channeling technique to analyze surface orientations of small crystallites. The

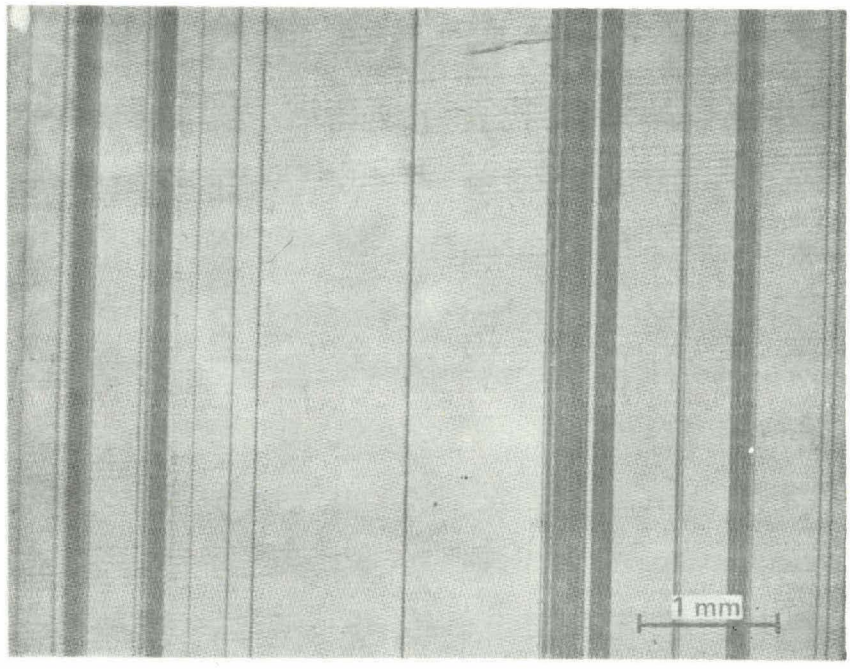

a

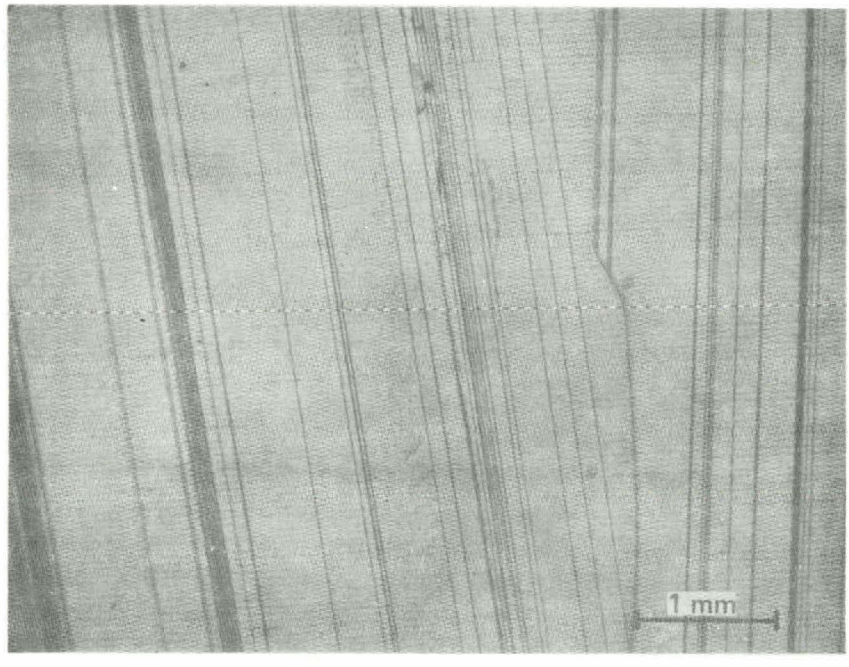

b

Fig. 4. Examples of typical twinning in ribbons grown with a carbon die: (a) parallel twinning and (b) non-parallel twinning and grain boundaries.

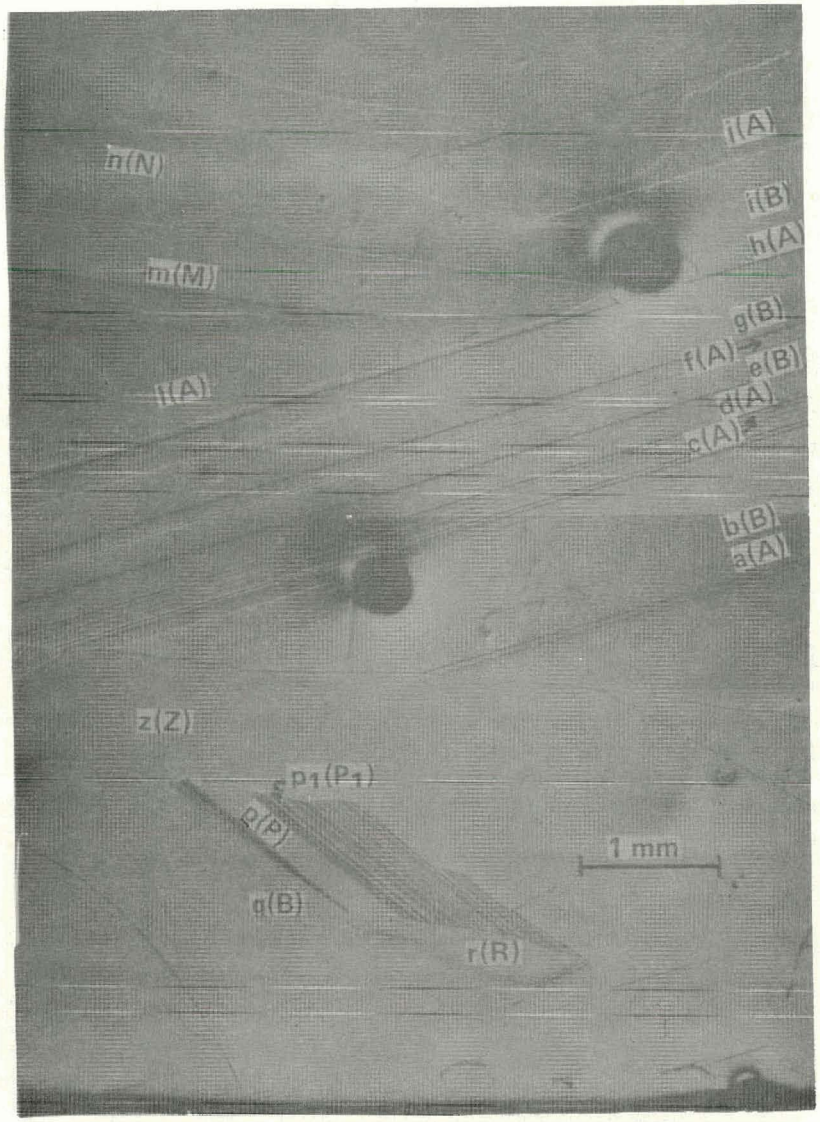

Fig. 5. **A ribbon section showing complexity of different surface features and twinning. a, b, c, -- refers to crystallite; A, B, -- refers to surface orientation.**

sample contains different grains, silicon carbide inclusions, and different types of twinning. All these defects can be encountered during ribbon crystal growing using carbon dies and, once analyzed, are readily interpreted through optical microscopy. For this reason, a thorough analysis is presented in the following section.

3.2 Analysis of <112> Twinning

Orientation analysis of crystal areas bounded by parallel lines in the <112> direction is summarized in Figs. 6a and 6b. Each figure shows a sequence of ECPs for each crystallite. One ECP covers only an angle of $\sim$ 6 degrees. Thus it is difficult to recognize the orientation pattern for crystal surfaces not being low-index surfaces. This difficulty is overcome by tilting the sample in steps of 6 degrees until the ECP on the screen can be matched with the computer-generated ECP. A sequence not larger than three ECPs is found sufficient to recognize the orientation of the sample in all cases.

The exact surface orientation of the sample is given by the center of the ECP obtained for zero sample tilt. Thus the orientation of the crystallite marked "a" in Fig. 5 and determined by the ECP sequence of Fig. 6a is in the neighborhood of the $[01\bar{1}]$ pole but tilted 10 degrees away from this pole. The ECP sequence of Fig. 6a indicates that this tilt is approximately along the (02?) lines. From the pole map given in Fig. 7 it follows that this position is near the lower periphery of the circle around the $[01\bar{1}]$ pole. A comparison of the ECP map (Fig. 6a) and of the pole map (Fig. 7) shows that (022) lines displayed in the ECP (Fig. 6a) go exactly parallel to the great circle through $[01\bar{1}]$, $[13\bar{3}]$, etc. Therefore, the true surface orientation

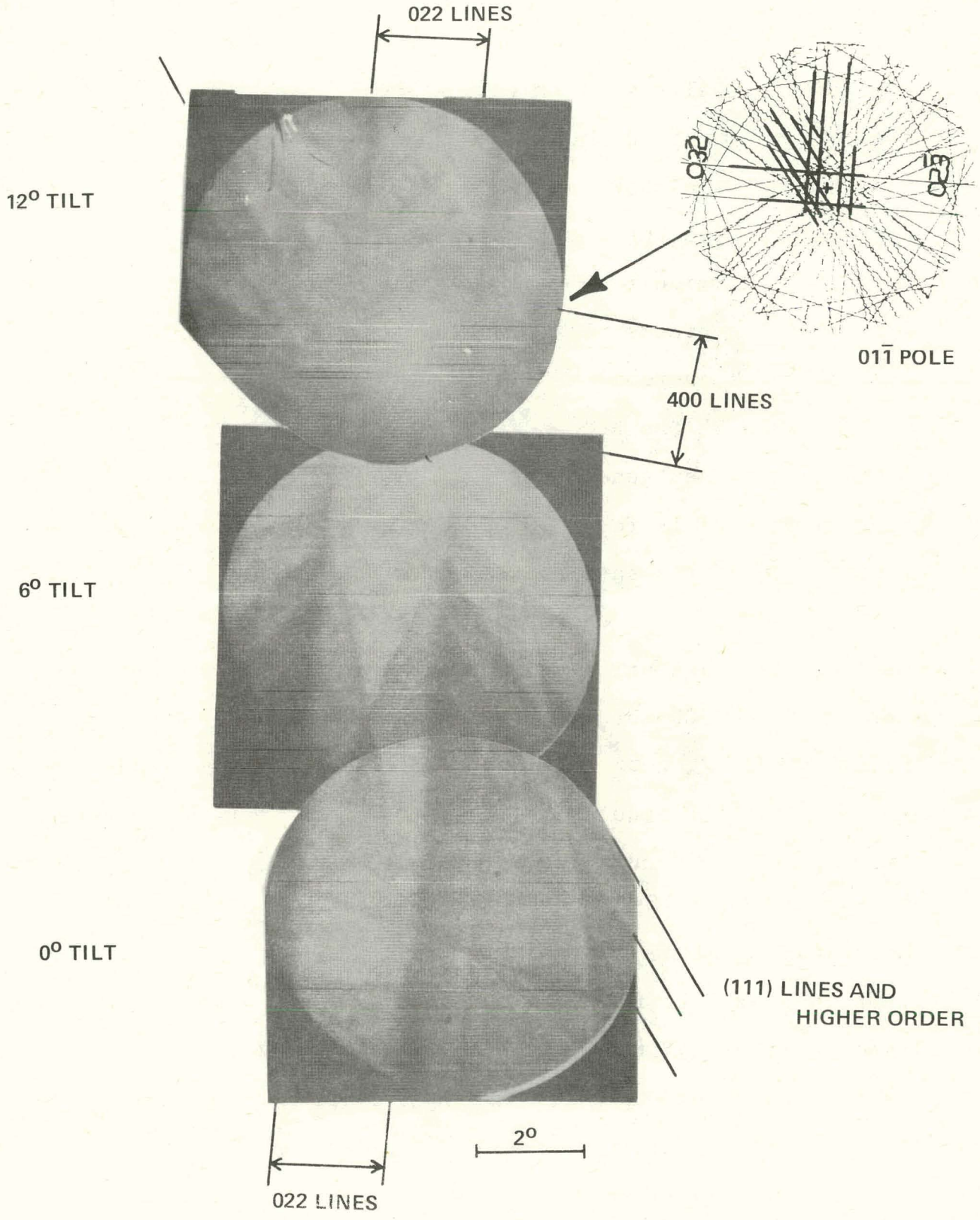

Fig. 6a. ECP sequence of crystallite "a" in Fig. 5.

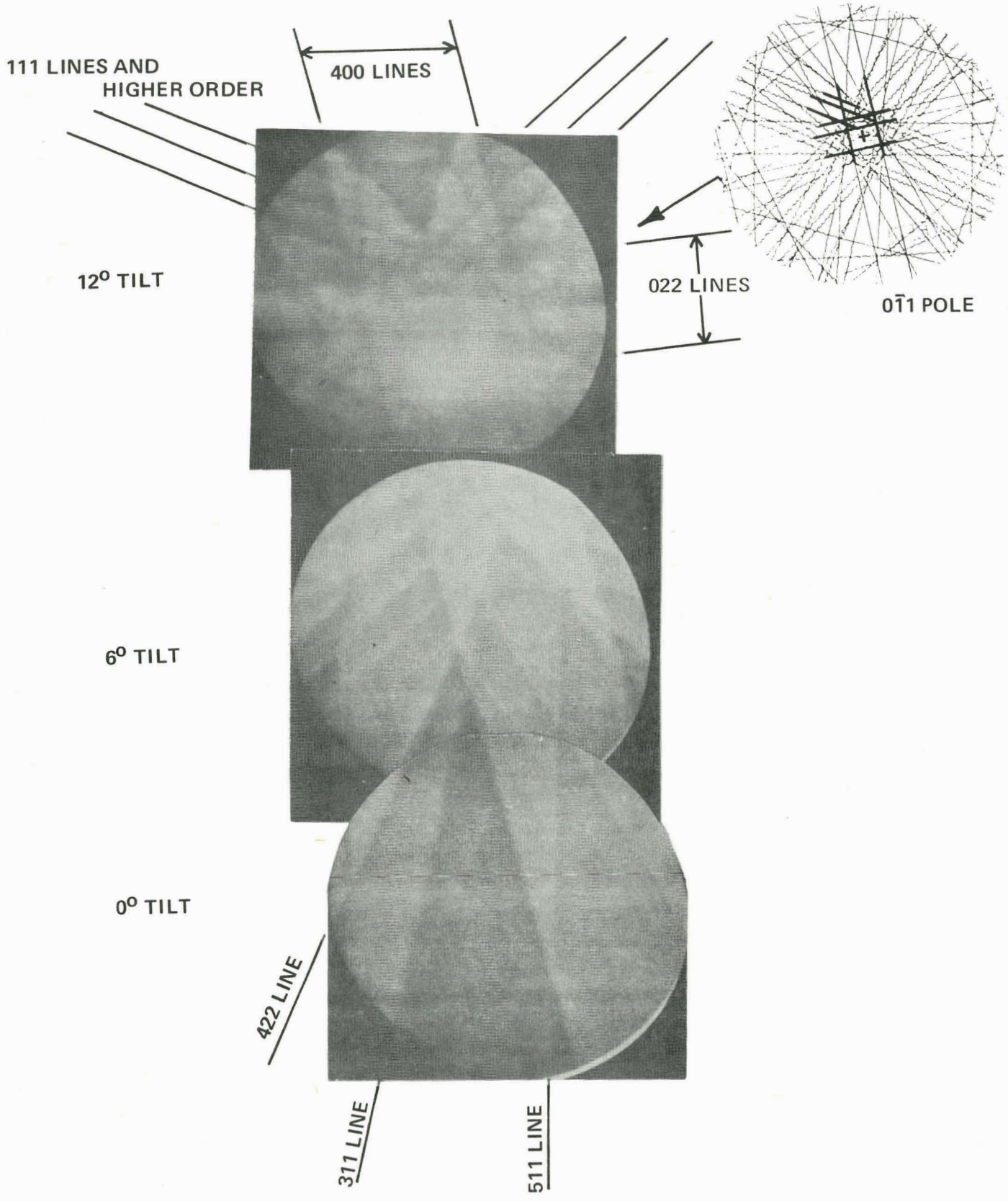

Fig. 6b. ECP sequence of crystallite "b" in Fig. 5.

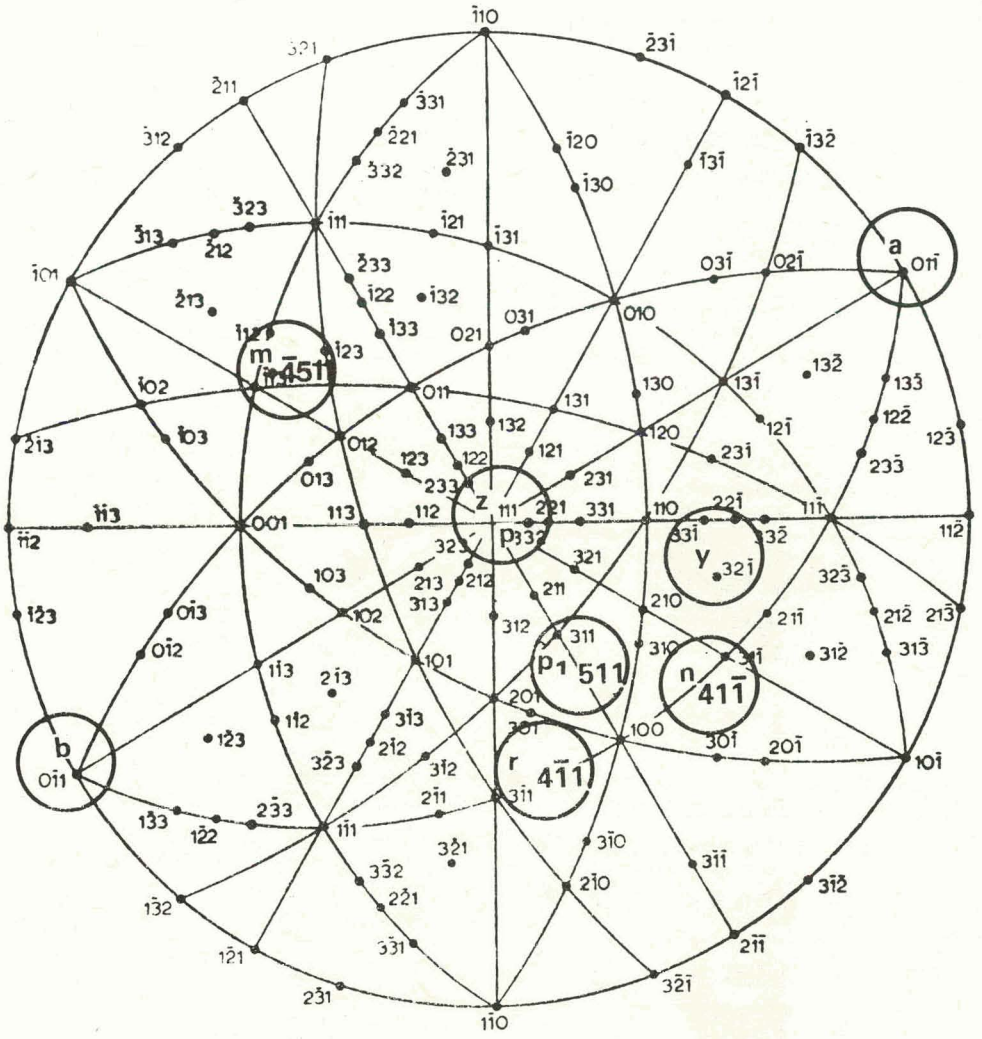

Fig. 7. **A [111] pole map indicating the surface orientation of different crystallites in Fig. 5.**

of crystallite "a" is tilted approximately 10 degrees away from the [01$\bar{1}$] direction towards the [11$\bar{1}$] pole.

Next we discuss the channeling pattern of the crystallite "b" shown in Fig. 5. Inspection of the ECP in Fig. 6b indicates that the surface orientation of this crystallite is again close to a <110> direction. However, note that this time the ECP reveals that the (022) lines are 70

degrees rotated relative to the (022) lines in the ECP of crystallite "a" in Fig. 6a. It follows, from the ECP sequence given in Fig. 6b, that the true surface orientation of crystallite "b" is tilted approximately 10 degrees toward a direction located between the [511] and [311] lines (see Fig. 6b). The exact direction is determined as follows. First we anticipate that the crystallites a and b are in a twin relationship and that twinning occurred on the (111) plane. Under such conditions, the surface orientation of b must be close to the $[0\bar{1}1]$ direction. Comparing the ECP in Fig. 6b and the pole map of Fig. 7, it follows that the great circle discussed in the analysis of crystallite "a" intersects the $[0\bar{1}1]$ pole in a direction which is 70 degrees rotated relative to the direction of the same circle through the $[01\bar{1}]$ pole. A great circle through the poles $[\bar{1}31]$, $[\bar{1}22]$, and $[\bar{1}13]$ would therefore indicate an identical direction through the $[01\bar{1}]$ pole. In addition, this circle would go parallel to the (411) channeling lines. As determined by the silicon "Structure Factor," however, these lines are forbidden reflections. Consequently, only the (511) and (311) lines are seen in the ECP of Fig. 6b. The true surface orientation of crystallite "b" is tilted 10 degrees towards the [411] direction between the [511] and [311] directions.

The orientation of the parallel strips labelled a to j in Fig. 5 alternates between the "A" and "B" surface orientation. The complete sequence of parallel twinning in the <112> direction is summarized as follows.

Surface	Twin Plane	Surface
$[01\bar{1}]$A	(111)	$[0\bar{1}1]$B
$[0\bar{1}1]$B	(111)	$[01\bar{1}]$A

Note that the twin lines are in the [112] direction and the (111) twin plane is perpendicular to the <011> ribbon surface.

3.3 Analysis of Non-Parallel Twinning

The crystallites labeled n and m in Fig.5 are bounded by lines of different directions. The ECP of crystallite n, given in Fig. 8a, indicates that the surface of n is close to a $[41\bar{1}]$ pole. Consulting the pole map given in Fig. 7, it follows that the surface of n is tilted approximately 10 degrees away from the $[41\bar{1}]$ pole. The ECP of crystallite j indicates a $[01\bar{1}]$ surface orientation. Thus the surface orientation of crystallite n is the result of $(11\bar{1})$ twinning of crystallite j. This reaction is summarized as follows.

Surface	Twin Plane	Surface
$[01\bar{1}]$J	$(11\bar{1})$	$[41\bar{1}]$N

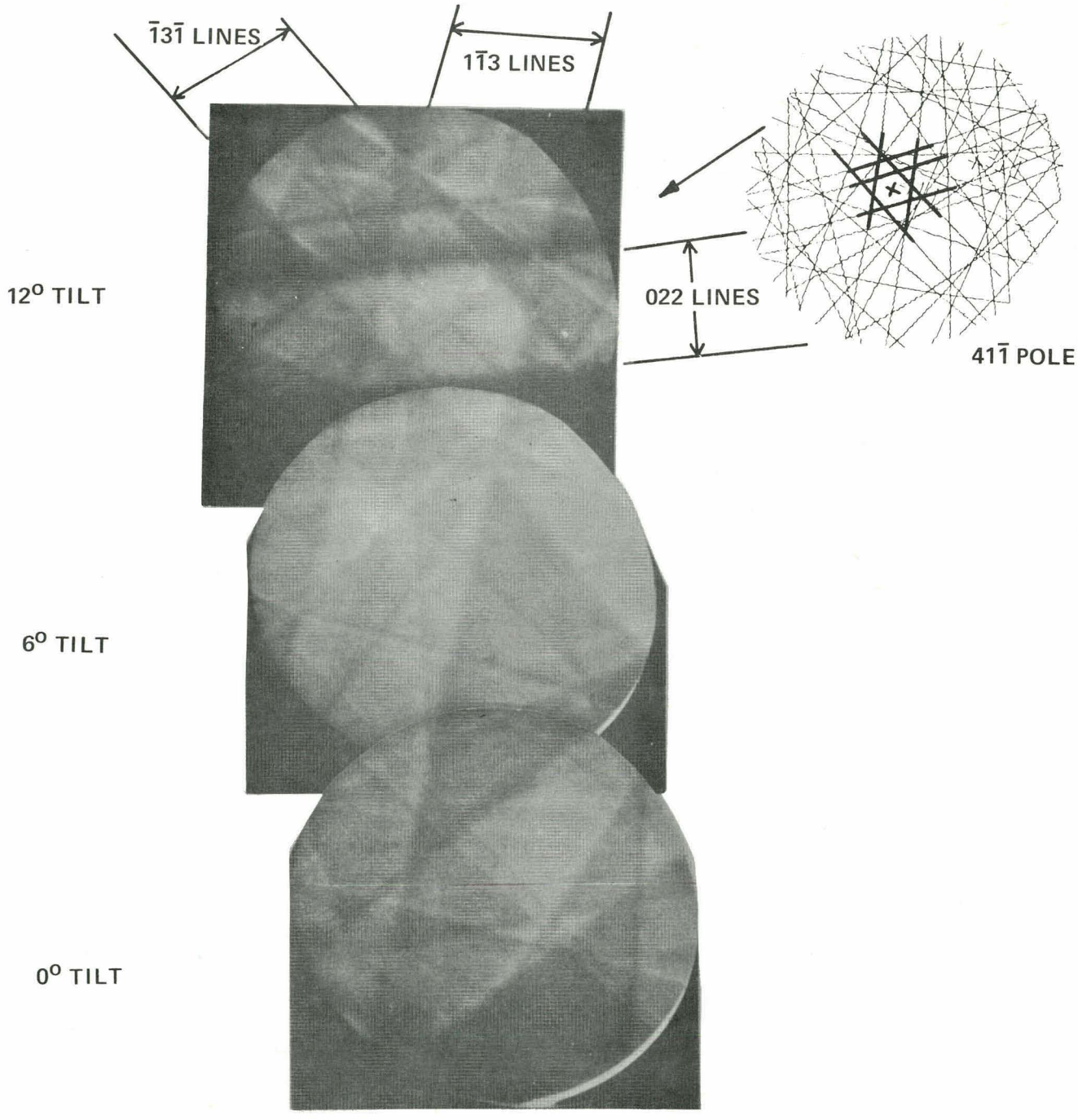

Fig. 8a. ECP sequence of crystallite "n" in Fig. 5.

The ECP of crystallite m is shown in Fig. 8b. The surface orientation of m is close to the [$\bar{1}$12] and [113] pole. With the help of the pole map (Fig.7) the twin reaction is analyzed as summarized below.

Surface	Twin Plane	Surface
[41$\bar{1}$]N	(111)	[$\bar{4}$ 5 11]M

The high-order orientation of m is calculated and fits the ECP orientation exactly (Fig. 8b). The boundary line between crystallites m and j (Fig. 5) corresponds to a change in orientation from [$\bar{4}$ 5 11] to [01$\bar{1}$] and cannot be explained by twinning. Consequently, this line is a grain boundary.

3.4 Analysis of Twin Lamellae

Another interesting subject for ECP analysis is the lamellae of closely spaced lines at position p in Fig.5. These lamellae are generated by double twinning as follows.

Surface	Twin Plane	Surface	Twin Plane	Surface
(111)P	($\bar{1}$11)	(511)P_1	($\bar{1}$11)	(111)P

The twinning occurs on the ($\bar{1}$11) plane, which is not perpendicular to the ribbon surface. The ECPs identifying this reaction are given in Figs. 9a, 9b, and 9c.

A complete orientation list of all crystallites labeled in Fig. 5 and analyzed through ECPs is given in Table I.

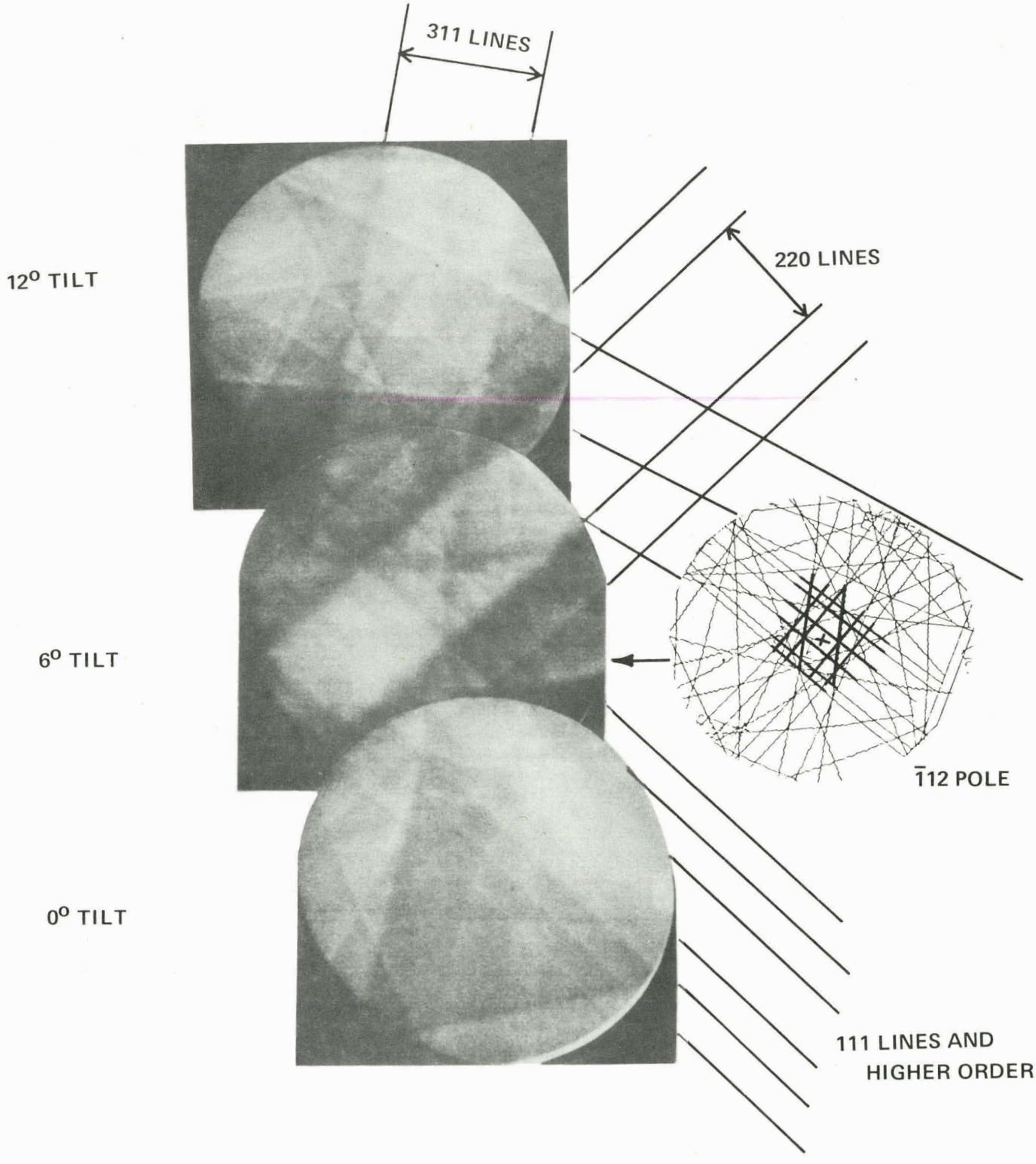

Fig. 8b. ECP sequence of crystallite "m" in Fig. 5.

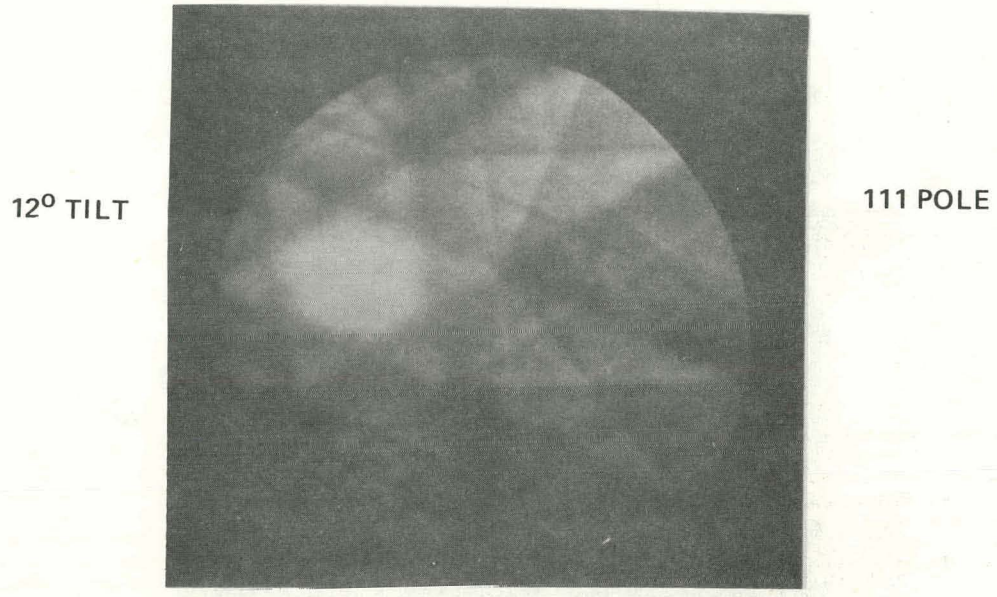

Fig. 9a. ECP sequence of crystallite "z" in Fig. 5.

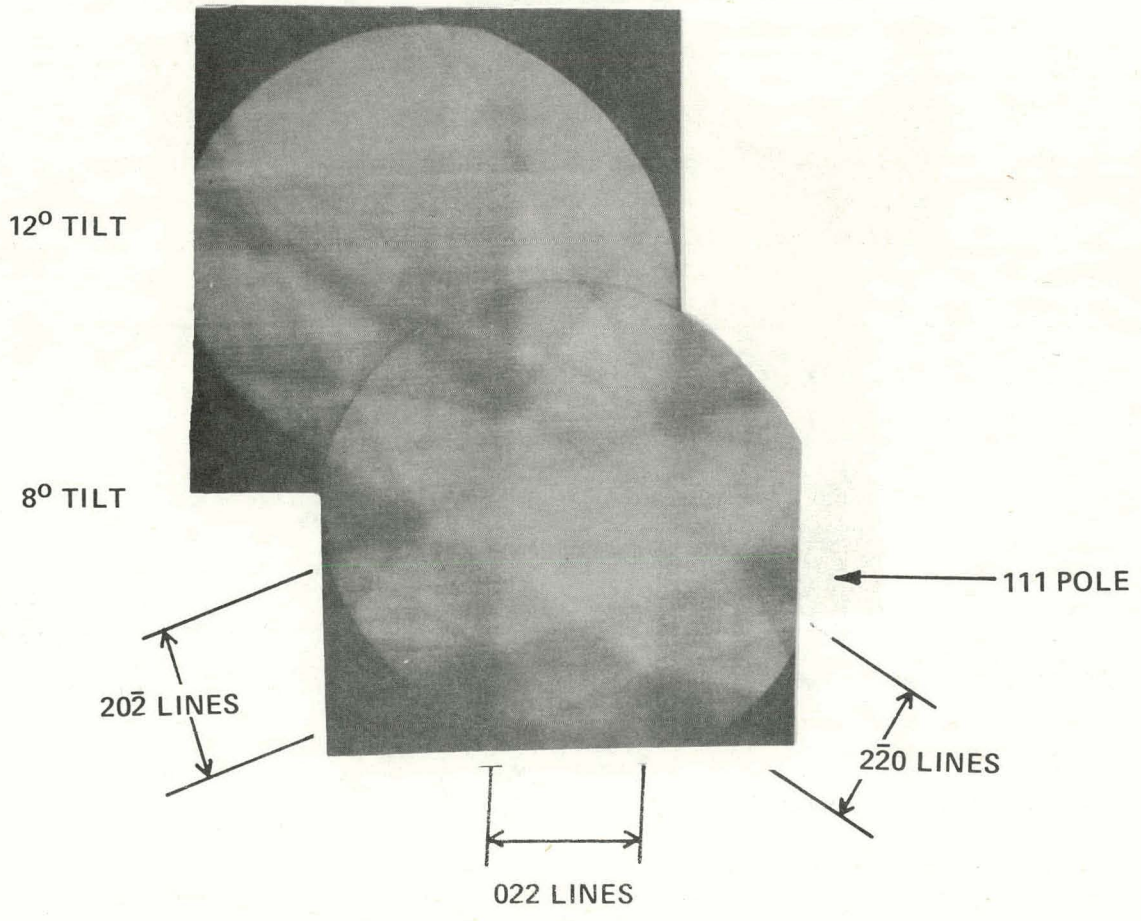

Fig. 9b. ECP sequence of crystallite "p" in Fig. 5.

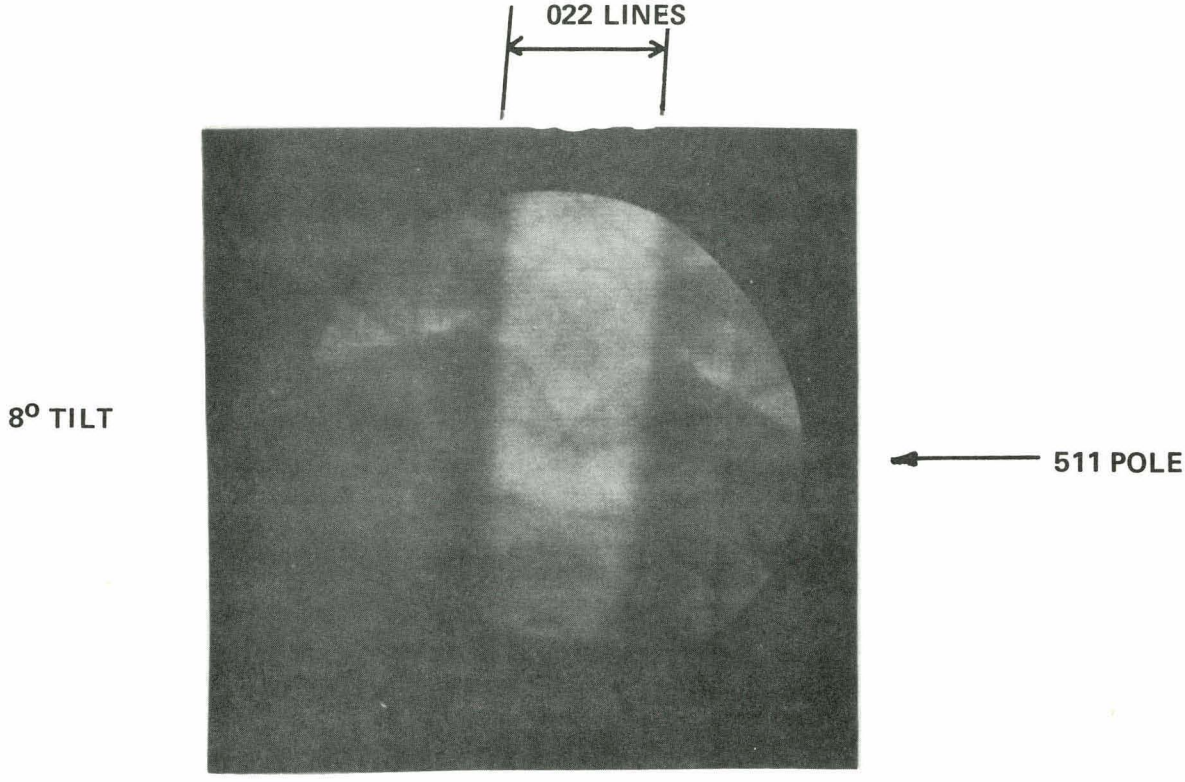

Fig. 9c. ECP sequence of crystallite "p_1" in Fig. 5.

TABLE I. Surface Orientation and Nature of Boundaries in Fig. 5

Type of Boundary	Surface Orientation	Twin Plane*	Nature of Boundary
A/B	$(01\bar{1})/(0\bar{1}1)$	$(111)_p$	Twin
A/N	$(01\bar{1})/(41\bar{1})$	$(11\bar{1})_i$	Twin
N/M	$(41\bar{1})/(\bar{4}\ 5\ 11)$	$(111)_i$	Twin
M/A	$(\bar{4}\ 5\ 11)/(01\bar{1})$		Grain boundary
Z/A	$(111)/(01\bar{1})$		Grain boundary
Z/p	$(111)/(111)$		Grain boundary
p/p_1	$(111)/(511)$	$(\bar{1}11)_i$	Twin
B/R	$(0\bar{1}1)/(4\bar{1}1)$	$(1\bar{1}1)_i$	Twin

*Subscripts p and i refer to twin plane perpendicular to and inclined to ribbon surface, respectively.

The non-parallel twinning leading to grain-boundary formation is the result of inclusions embedded during ribbon growth into the ribbon surface. Such inclusions were previously identified as SiC particles (Quarterly Technical Progress Report Number 2). The inclusions causing twins and grain boundaries (Fig. 5, position I) are shown in the SEM micrographs of Fig. 10.

3.5 Analysis of Steady-State Grown Ribbon Surfaces

In general, surface-orientation patterns of ribbons - once steady-state growth conditions have been achieved - are considerably simpler than those discussed in the previous section. At present, it is not possible to control the "seeding operation" sufficiently to influence the surface orientation of the ribbon grown during steady state. Because of silicon carbide formation during seeding, the original seed/crystal relation is rapidly lost and the final ribbon quality is mostly dominated by twin lines in the <112> direction. An x-ray topograph of a typical crystal-seed interface is given in Fig. 11 and shows clearly the catastrophic collapse of seed orientation due to heavy twinning. All twins inclined towards the growth direction grow out relatively fast. If the inclusion of silicon carbide particles in the ribbon surface can be avoided, steady-state growth is dominated by surface orientations close to a <110> direction.

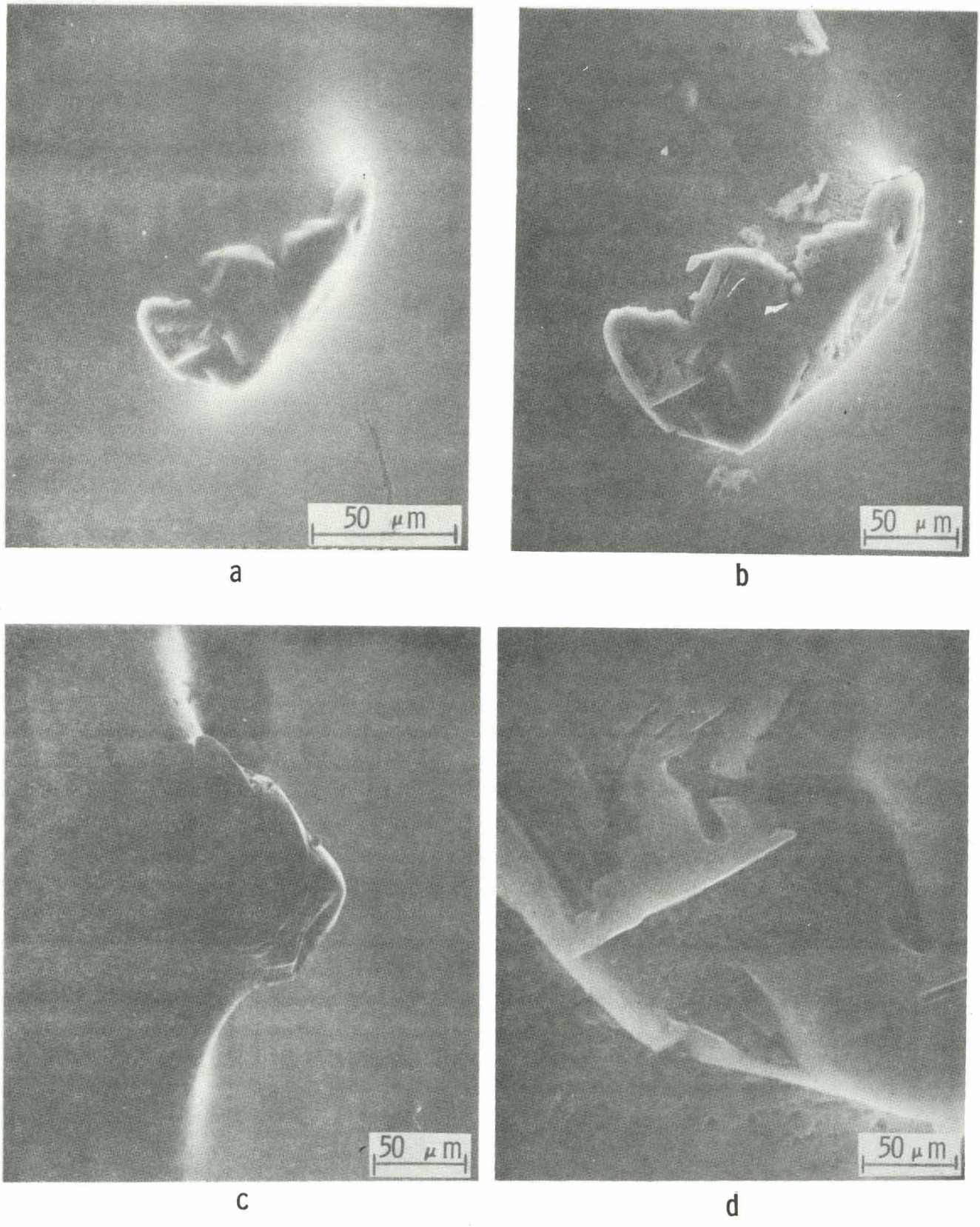

Fig. 10. SEM micrographs of a SiC particle : (a) before etching, (b) after 10-sec Sirtl etch, (c) closeup view of etched area in and around particle, (d) view of etched area showing surrounding unetched walls of SiC.

Fig. 11. An x-ray topograph of a typical crystal-seed interface showing the catastrophic collapse of seed orientation due to heavy twinning.

To define the surface orientation of ribbons grown under steady-state conditions, we introduce the convention summarized in Fig. 12. Accordingly, the angle between the growth direction and the twin boundaries is called α. The resultant tilt angle, θ_r, gives the actual surface orientation of the ribbon. This surface orientation is measured as a misorientation against the [011] direction and has the two components θ_g and θ_a, where θ_g is the tilt along the growth direction and θ_a is the tilt around the growth direction perpendicular to it.

Table II summarizes typical surface orientations obtained for different seed orientations. On the basis of these and other results, we conclude that control of surface orientation of ribbons grown under steady-state conditions does not, at present, exist. It can be noted that surface misalignment covers a range between 5 and 15 degrees against the [011] surface. Ribbons with twin planes inclined almost perpendicular to the surface and a surface tilt of $\theta_r = \theta_a = 8$ degrees (with $\theta_g = 0$) have been grown. For such ribbons the twin boundaries are parallel to the [21$\bar{1}$] growth direction.

Figure 13 gives an example of such a ribbon and its surface analysis. Figure 14 shows the more general case - double tilt - for the ribbon. Note that both

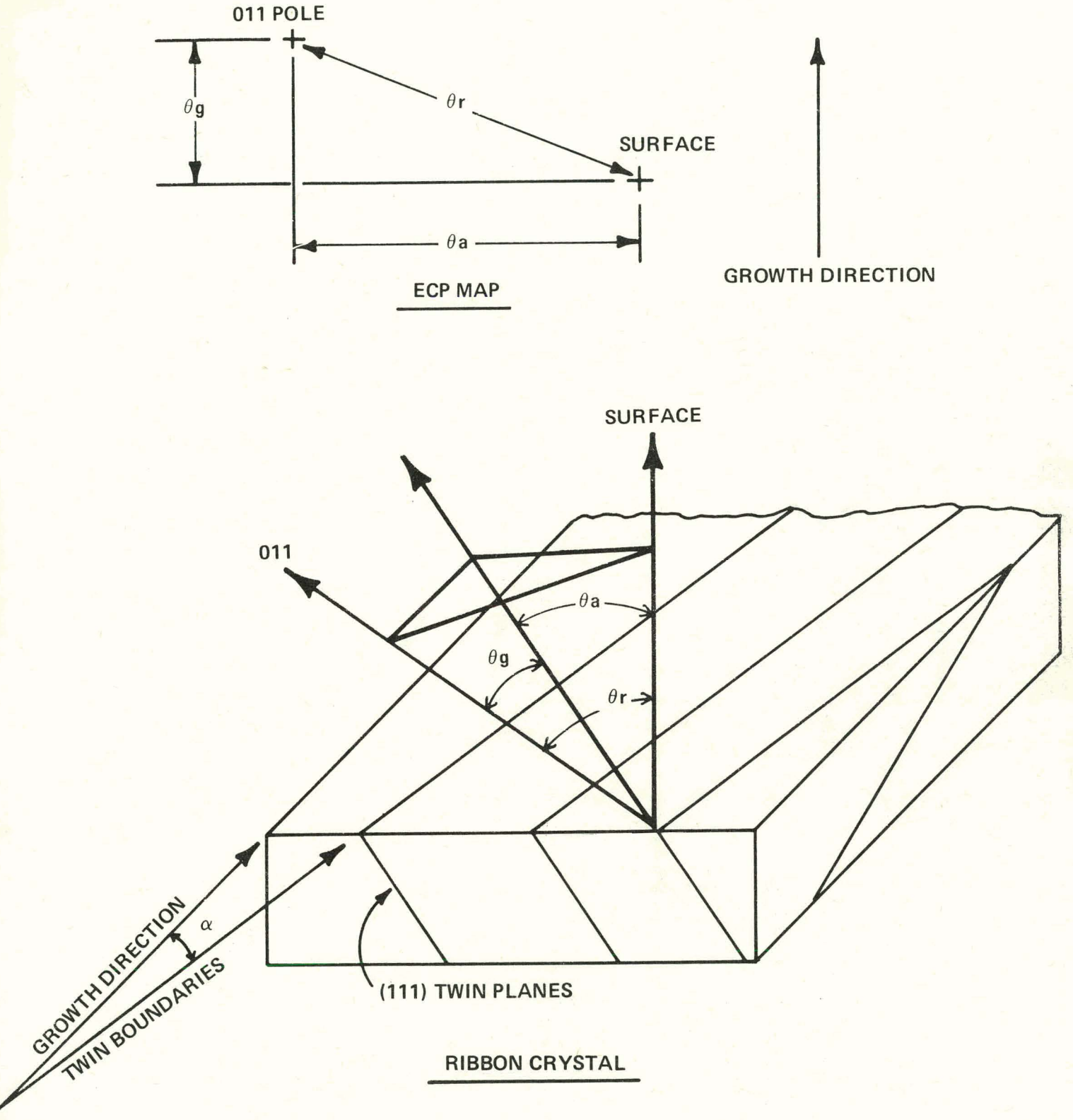

Fig. 12. A schematic drawing of a ribbon crystal with misorientation θ_r against the [011] direction.

TABLE II. Steady-State Growth of Ribbon

Ribbon Number	Seed Orientation		Sample Distance from Seed (cm)	Sample Orientation			Twin Axis a/b	Remarks
	Face	Growth Direction		Face				
				Nearest Pole	Deviation (degrees)	Growth Direction		
40404	(111)	$\langle\bar{1}\bar{1}2\rangle$	>50	011	$\theta_R = 11.3$ $\theta_a = 3.5$ $\theta_g = 10.7$	$2\bar{1}\bar{1}$	$11\bar{1} \leftrightarrow \bar{1}\bar{1}1$	Twin boundaries in growth direction
40812	$(1\bar{1}0)$	$\langle 111\rangle$	50	011	$\theta_R = 9.7$ $\theta_a = 5$ $\theta_g = 8.3$	$21\bar{1}$	$1\bar{1}1 \leftrightarrow \bar{1}1\bar{1}$	Twin boundaries not in growth direction (10^o off)
40820	$(1\bar{1}0)$	$\langle 111\rangle$	50	011	$\theta_R=\theta_a=8.4$ $\theta_g = 0$	$21\bar{1}$	$1\bar{1}1 \leftrightarrow \bar{1}1\bar{1}$	Twin boundaries in growth direction
50520	(100)	$\langle 110\rangle$	120	011	$\theta_R = 18$ $\theta_a = 14$ $\theta_g = 11$	$21\bar{1}$	$1\bar{1}1 \leftrightarrow \bar{1}1\bar{1}$	Twin boundaries in growth direction

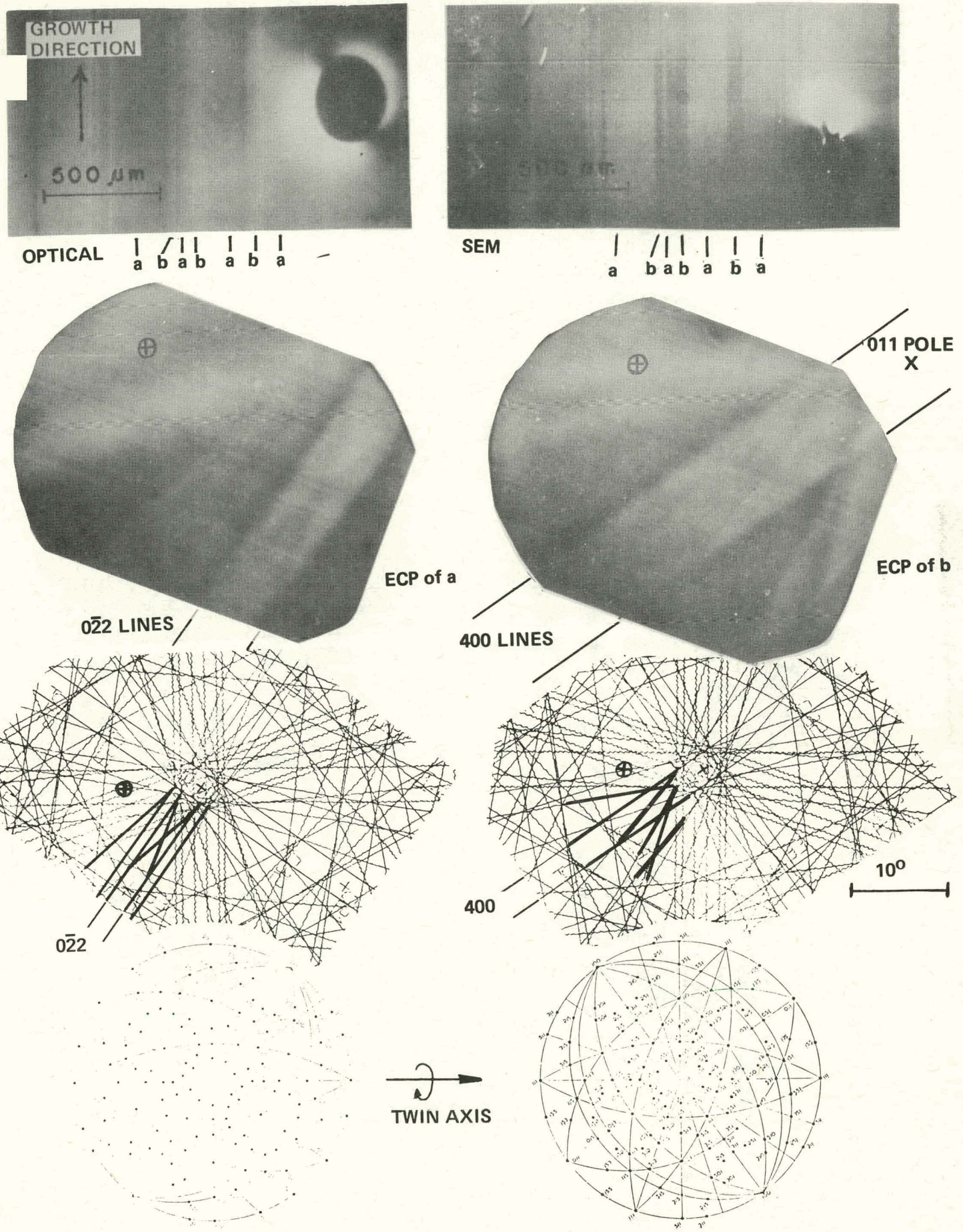

Fig. 13. Orientation analysis of a ribbon with twin boundaries parallel to the growth direction, i.e., $\theta_g = 0$.

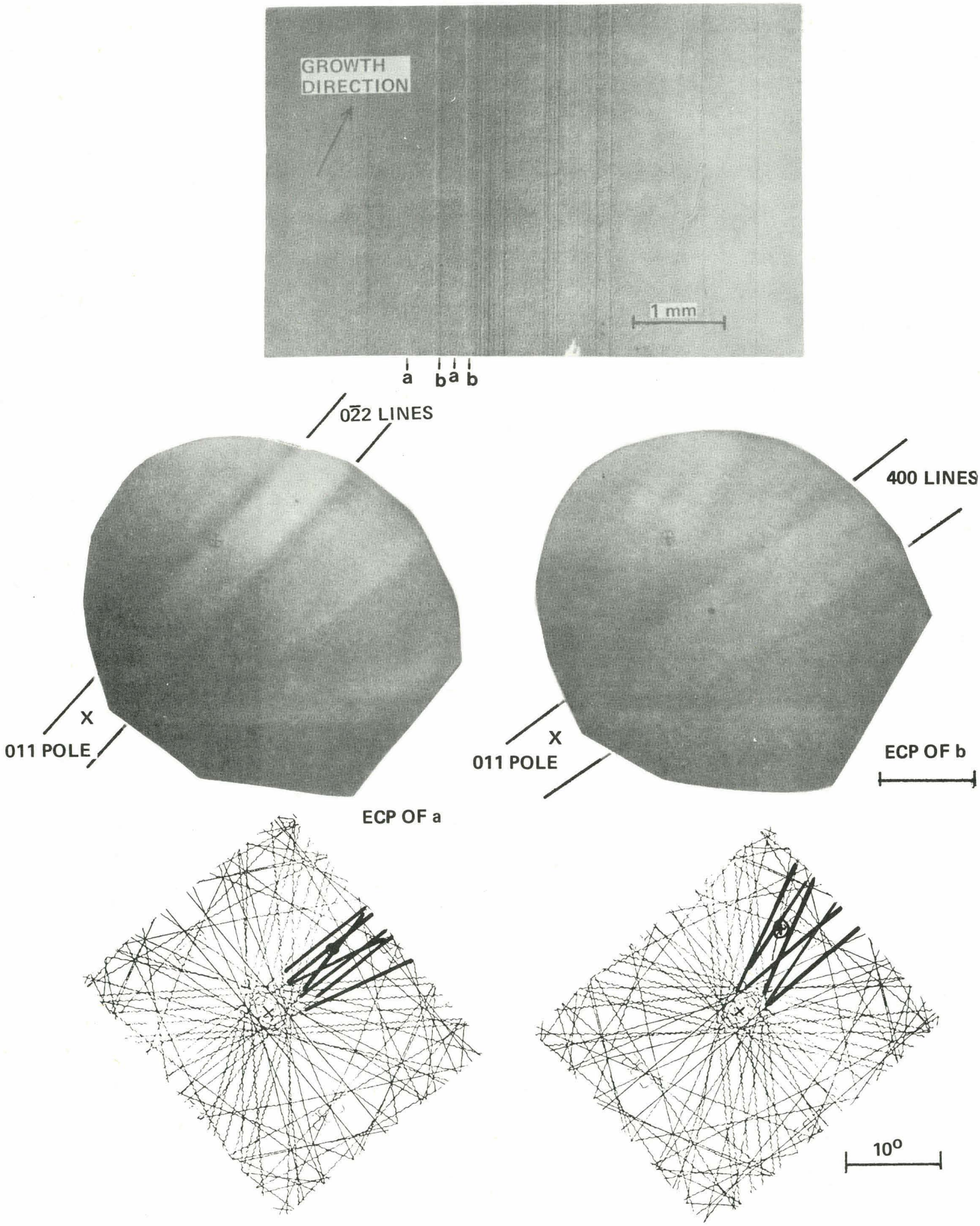

Fig. 14. Orientation analysis of a ribbon with twin boundaries non-parallel to the growth direction, i.e., $\theta_g \neq 0$.

ribbons (analyzed in Figs. 13 and 14) were grown with the same seed orientation and that steady-state orientation was measured at the same distance from the seed.

4. SUMMARY

The technique of electron channeling was applied to determine surface orientation of ribbon crystals. The results indicate that surfacc orientation of ribbons established under steady-state growth conditions approaches the [011] orientation. Single- and double-tilt misalignments off the [011] direction occur. The best ribbon obtained showed approximately 5 to 8° single tilt and twin boundaries exactly in the [21$\bar{1}$] growth direction. Seed orientation has no influence on final surface orientation.

5. REFERENCES

1. P. B. Hirsch and C. J. Humphries, in Scanning Electron Microscopy/1970, IITRI, p. 449, Chicago, I11. (]970).

2. Technical Report No. 6, ARPA Contract No. DAHC-15-72-C-0274, G. H. Schwuttke, Principal Investigator, July 1975.

COMPARISON AND PROJECTION OF SINGLE- VERSUS MULTIPLE-RIBBON TECHNOLOGY

by

A. Kran

1. INTRODUCTION

Photovoltaic energy conversion faces some general decisions in which its technological prospects are the major issue. At the silicon sheet material level, the situation is similar. Thus, explicit information to improve prediction must be generated as soon as possible. The difficulty with preparing a "firm" technological forecast is that today's data, both technical and economic, are still "soft" and often unstructured. Technology and manufacturing capability is being projected from a research vantage point, which is an elusive task.

At this point, our outlook for low-cost silicon sheet growth can be characterized as guarded optimism, with an option to reassess the situation each time relevant technology milestones are approached. This is one reason for developing tools and capabilities for automatic computation and conversion of unstructured data, as the data become available, into analyzable procedures with explicit assumptions, using mathematical models and computer simulation techniques that are readily validated.

In this report, single- and multiple-ribbon growth systems are compared for their ability to provide low-cost silicon

sheet material. The comparison is based on a production unit concept, technology projection, and sensitivity analysis. The growth system chosen is further analyzed to identify those development tasks which will maximize the reduction of silicon sheet material cost.

2. THE PRODUCTION UNIT CONCEPT

The production unit concept reduces the complexity of interaction among processing sectors in a manufacturing operation. It has been chosen, in conjunction with technology forecasting and sensitivity analysis, for studying the future prospects of low-cost silicon sheet material.

A production unit may be thought of in terms of three elements: processing technology, resources, and raw materials. The two production units defined for this analysis deal with the transformation of polycrystalline bulk silicon into ribbons or sheets of single or near-single crystal material, suitable for subsequent solar-cell fabrication. They are described as a specific combination of manpower, crystal-growing equipment, and polycrystalline silicon needed to progress through the crystal-pulling sector in a solar-cell manufacturing operation.

Both production units use Czochralski type crystal pullers, modified for growing ribbon silicon by means of the capillary

action shaping technique (CAST), but are distinguished by their approaches to implementing a low-cost silicon sheet material program as follows:

1. Relatively simple, single-ribbon growth process and equipment, characterized by automatic melt replenishment and continuous, unattended growth.

2. Highly complex, multiple-ribbon growth process and production equipment system, aimed at large-volume per unit time production.

3. COMPUTER SIMULATION MODEL OF THE PRODUCTION UNIT

Interactive computer simulation models are being designed to support the development of technological and economic data required to define the potential of silicon sheet growth for large-scale photovoltaic applications. One of these models, representing a generalized silicon ribbon growth production unit, was recently completed (see Quarterly Technical Progress Report Number 1). It simulates the complex interactions between physical variables pertaining to silicon ribbon processing and the economic parameters associated with product manufacturing and business management.

The mathematical model requires 14 equations and some 23 parameters to describe. The computer simulation model is

basically deterministic and can be readily validated. It is coded in a scientific programming language (APL) and executed on a time-shared computing system.

New input or changes to stored parameter values are provided to the model by the user, under program control, in real-time and an interactive mode, from a terminal remotely located with respect to the computing system. Input data sets created in this manner can be used for immediate calculation and display of results, or stored for subsequent manipulation. The rapid-iteration feature of the model has made it a most useful tool for the data-collection phase of this study, particularly for the sensitivity analysis, where many data points are needed for plotting trends.

Input parameters to the model are grouped as follows. A ribbon data category contains processing-related parameters, such as ribbons grown simultaneously, width, growth rate, thickness, and percent yield of material suitable for solar-cell fabrication.

A direct-cost category comprises crystal-growth system cost, equipment life and interest rate, so that equipment capital recovery can be calculated, and equipment availability. The latter parameter is defined as the percent of time the system is available for crystal pulling, excluding setup, polysilicon melt-down, and random machine failure time. Also included here are the direct personnel required to assure

efficient operation of the system. Three classifications - technician, engineer, and supervisor - are defined in terms of their respective salaries and of the fraction of their time charged to the operation of the production unit. Furthermore, polysilicon cost, the percent yield of polysilicon to ribbon, and services and supplies, which include die cost, complete the list of specifically named items. The remainder - overhead, general and administrative expenses, and profit - are defined as percentages relating to other direct-cost items.

A miscellaneous category defines the workweek in terms of hours and of energy-conversion efficiency at AM1, a hypothetical value to assess energy capacity cost at the level of silicon sheet material.

Output from the model consists of the major factors contributing to sheet material and energy capacity cost. They include the average yielded growth rate, the resultant yield factor, plus the following direct cost elements, calculated in dollars/m^2: equipment capital recovery, personnel cost, polysilicon cost, and services and supplies. Also calculated in dollars/m^2 are overhead cost, G&A expense, and profit. The addition of these items results in a total dollars/m^2 figure for silicon sheet material, representing a selling price to a manufacturer, or purchase cost to a potential buyer.

4. TECHNOLOGY PROJECTION - SINGLE- VS MULTIPLE-RIBBON GROWTH SYSTEMS

4.1 General

Our approach to an assessment of future technology capability consists of assigning a set of parameters which represent our "baseline", or current state-of-the-art, to the production unit model. As technology milestones are met, the baseline is updated. When experimental information is not available, such as in the case of multi-ribbon growth, a conservative estimate is substituted as the baseline. The business-related data, such as overhead and G&A, are intended to be representative of a typical small-to-medium-size concern.

All technology projections are made from the baseline. For this analysis, two projections, representing intermediate and future points in time, were made for both the single- and multiple-ribbon growth systems. To maximize compatibility between forecasts for the two systems, only those parameters pertaining directly to the respective systems were projected independently. Figure 1 lists those variables and their assigned values which are used for both single- and multiple-ribbon growth systems. The three values represent the baseline, a transition period estimate, and the future. Corresponding information is provided in Table I, which highlights the difference between the two production units. It also groups

```
  RIBBON DATA FROM SIMULATIONS 1 4 5 DATED 03/02/76
3  RIBBON GROWTH RATE,M/HR -    1.50  2.49  3.59 ..OR AS PCT  30  40  5(
4  RIBBON THICKNESS, MM -  0.30 0.20 0.15
5  YIELD OF "CELL QUALITY" RIBBON, PCT -    70  80  90

   DIRECT COST
7       EQUIPMENT LIFE, YEARS -    7.0  8.0 10.0
8       INTEREST RATE, PERCENT -  10.0 10.0 10.0
   PERSONNEL PER SHIFT PER MACHINE
10 11 NO. OF SUPVS -   0.05 0.05 0.05 AT $ -  25000 25000 25000
12 13 NO. OF ENGRS -   0.10 0.10 0.10 AT $ -  20000 20000 20000
14 15 NO. OF TECHN -                  AT $ -  10000 10000 10000
16 POLY SILICON COST, DOLS/KG -    65  45  30
17 POLY YIELD TO RIBBON,PERCENT -    80  85  90
   SERVICES AND SUPPLIES
18      CRUCIBLE/DIE/PARTS COST PER  WEEK-  150 125 100 DOLLARS
19      POWER COST AT -  0.05 0.05 0.05 DOLLARS PER KWH
20      ENERGY TO OPERATE EQUIPMENT -    12  11  10 KW

21 22  O/H -    50  50  50 PCT OF PERS+    10  10  10 PCT OF RAW MATL COST
23  G_AND_A -    10  10  10 PERCENT OF DIRECT COST+OVERHEAD

24  PROFIT BEFORE TAX, PERCENT - 10 10 10 OF DC+O/H+G&A

   MISCELLANEOUS
25 WORKWEEK, HOURS -   168 168 168
26 CONVERSION EFFICIENCY, PERCENT -    8.00 10.00 12.00
27 ENERGY DENSITY AT AM1,KW/SQ M PEAK -     1   1   1
```

Fig. 1. List of jointly-used ribbon parameters and their assigned values.

TABLE I. Technology Projection List of Production Unit Parameters

Processing Technology	Single-Ribbon Growth System			Multiple-Ribbon Growth System		
	Present	→	Future	Present	→	Futur
Ribbon width (cm)	2.5	5.0	10.0	2.5	3.0	5.0
Simultaneous ribbons	N/A	N/A	N/A	1	2	3
Growth rate (% of max)	30	40	50	30	40	50
Ribbon thickness (mm)	0.30	0.20	0.15	0.30	0.20	0.15
Resources						
Ribbon puller ($)	50,000	25,000	20,000	175,000	150,000	125,0
Availability (% of time)	70	80	90	60	70	80
Technicians (No.)	0.50	0.25	0.15	1	1	1
Raw Materials						
Polysilicon cost ($)	65	45	30	60	45	30

production unit parameters into three major elements - processing technology, resources, and raw material - which will be disussed next.

4.2 Processing Technology

Major components of processing technology are ribbon width and growth-rate capability.

With the use of a single-ribbon growth system, 2.5-cm-wide ribbons are routinely pulled, 5-cm-wide ribbons can be envisioned, and 10-cm-wide ribbons are projected for the future. For multiple-ribbon growth systems, forecasting is more difficult, as instrumentation and control requirements are known to be more complex. More important, no successful multiple-ribbon growth has yet been reported. Consequently, a maximum of three ribbons grown simultaneously, each about 5 cm wide, is projected and related, in terms of difficulty, to a 10-cm-wide single ribbon.

Accordingly, two options must be evaluated for their effect on silicon sheet material cost: 10-cm-wide ribbons achieved through single-ribbon growth, and a 15-cm-wide capability attained through growing three simultaneous ribbons, each 5 cm wide.

Growth-rate capability is anticipated to be the same for

single- as for multiple-ribbon growth systems. At present, 0.3-mm-thick ribbons are pulled at 1.5 m/hr, which is 30% of the theoretical maximum growth rate.

For large width-to-thickness ratios, the theoretical maximum growth rate has been shown (1) to vary inversely as the square root of ribbon thickness. Figure 2 provides a graphical representation of our projected growth rate increase from 30 to 50% of theoretical maximum, coupled to a corresponding decrease in ribbon thickness from 0.3 to 0.15 mm. However, it appears that separate development efforts will be required to meet the individual objectives of ribbon thickness and growth rate.

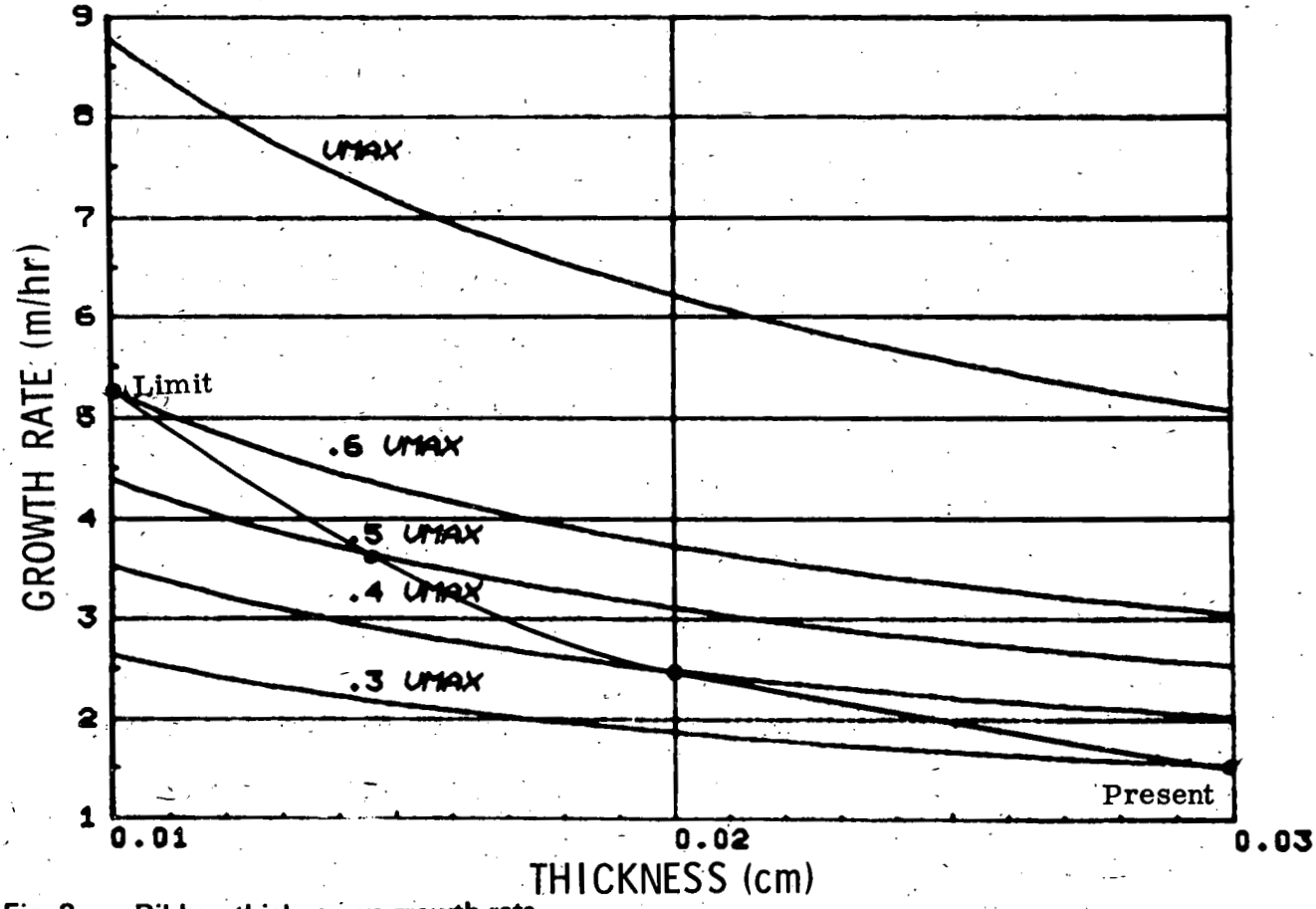

Fig. 2. Ribbon thickness vs growth rate.

4.3 Resources

A single-ribbon growth system can be implemented through modification of commercially available Czochralski type crystal-pullers at a total cost of about $50,000. Assuming a significant future market for photovoltaic products, a proportionately large market is envisioned for ribbon-growth systems, which implies that they could be standardized, mass-produced, and sold as special-purpose equipment for about $20,000. Such systems are expected to be highly reliable, featuring machine availability of up to 90%. Fully automated, the systems also would reduce the amount of required manpower to the point where one technician could operate on the order of ten systems.

Because of the significantly greater complexity of multi-ribbon growth production systems, a more modest potential for cost improvement is anticipated. From today's estimated capital cost of $175,000, a decrease to $125,000 might be realistic, with an increase in system availability from 60 to 80%. Required manpower is assumed to remain constant at one technician full time.

4.4 Raw Material

The cost of polycrystalline silicon in bulk form has remained unchanged at about $65/kg for a number of years. A considerably larger market for this material should lead to an estimated decrease in price to about $30/kg.

4.5 Result of Technology Projection

A list of input parameters and the resultant ouput of the two production units are given in Fig. 3 and Table II and in Fig. 4 and Table III. Figure 5 summarizes the information in graphical form, comparing cost at the silicon sheet material level. For the single-ribbon growth system, this cost decreases from the baseline value of $\$678/m^2$ to $\$38/m^2$ in

```
  RIBBON DATA FROM SIMULATIONS 1 4 5 DATED 03/02/76
1  RIBBONS GROWN SIMULTANEOUSLY -     1    1    1
2  RIBBON WIDTH, CM -    2.5   5.0 10.0
3  RIBBON GROWTH RATE,M/HR -    1.50   2.49   3.59 ..OR AS PCT   30   40   50
4  RIBBON THICKNESS, MM -  0.30 0.20 0.15
5  YIELD OF "CELL QUALITY" RIBBON, PCT -    70   80   90

   DIRECT COST
6  RIBBON FURNACE, DOLLARS -    50000   25000   20000
7      EQUIPMENT LIFE, YEARS -    7.0   8.0 10.0
8      INTEREST RATE, PERCENT -   10.0 10.0 10.0
9      EQUIPMENT AVAILABILITY, PERCENT -     70    80    90
   PERSONNEL PER SHIFT PER MACHINE
   11 NO. OF SUPVS -   0.05 0.05 0.05 AT $ -   25000 25000 25000
12 13 NO. OF ENGRS -   0.10 0.10 0.10 AT $ -   20000 20000 20000
14 15 NO. OF TECHN -   0.50 0.25 0.15 AT $ -   10000 10000 10000
16 POLY SILICON COST, DOLS/KG -    65   45   30
17 POLY YIELD TO RIBBON,PERCENT -    80   85   90
   SERVICES AND SUPPLIES
18     CRUCIBLE/DIE/PARTS COST PER  WEEK-   150 125 100 DOLLARS
19     POWER COST AT -   0.05 0.05 0.05 DOLLARS PER KWH
20     ENERGY TO OPERATE EQUIPMENT -    12   11   10 KW

21 22  O/H -    50   50   50 PCT OF PERS+    10   10   10 PCT OF RAW MATL COST
23  G_AND_A -    10   10   10 PERCENT OF DIRECT COST+OVERHEAD

24  PROFIT BEFORE TAX, PERCENT - 10 10 10 OF DC+O/H+G&A

   MISCELLANEOUS
25 WORKWEEK, HOURS -   168 168 168
26 CONVERSION EFFICIENCY, PERCENT -    8.00 10.00 12.00
27 ENERGY DENSITY AT AM1,KW/SQ M PEAK -     1    1    1
```

Fig. 3. List of single-ribbon parameters and their assigned values.

the future. The corresponding values for multiple-ribbon growth systems range from $\$1292/m^2$ to $\$59/m^2$, which is higher by almost a factor of two. Because of both the higher cost of silicon sheet material and the greater complexity of the multiple-ribbon growth system, the analysis favors single-ribbon growth. Next, a sensitivity analysis of the three production unit elements will be undertaken to enhance the single- vs multiple-ribbon system considerations.

TABLE II. Economics of Silicon Ribbon - One Single-Ribbon Puller

Simulation Date and No. 03/02/75	1	4	5
Ribbons grown simultaneously	1.00	1.00	1.00
Ribbon width (cm)	2.50	5.00	10.00
Average yielded growth rate (sq m/hr)	0.02	0.08	0.29
Combined yield factor	0.56	0.68	0.81
Direct cost (dollars/sq meter)			
Equipment capital recovery	66.54	7.01	1.33
Personnel	224.49	36.13	8.17
Polysilicon cost	81.13	30.84	12.94
Services/supplies	71.45	14.88	3.60
Subtotal:	443.61	88.86	26.04
Overhead cost (dollars/sq meter)	116.79	20.16	5.13
G&A expenses (dollars/sq meter)	56.04	10.90	3.12
Profit (dollars/sq meter)	61.64	11.99	3.43
Total cost (dollars/sq meter)	678.08	131.92	37.72
Dollars per kw	8476.03	1319.22	314.36

```
  RIBBON DATA FROM SIMULATIONS 6 7 8 DATED 03/02/76
1  RIBBONS GROWN SIMULTANEOUSLY -     1   2   3
2  RIBBON WIDTH, CM -    2.5  3.0  5.0
3  RIBBON GROWTH RATE,M/HR -    1.50  2.49  3.59 ..OR AS PCT  30  40  50
4  RIBBON THICKNESS, MM -  0.30 0.20 0.15
5  YIELD OF "CELL QUALITY" RIBBON, PCT -    70  80  90

  DIRECT COST
6  RIBBON FURNACE, DOLLARS -  175000 150000 125000
7      EQUIPMENT LIFE, YEARS -    7.0  8.0 10.0
8      INTEREST RATE, PERCENT -  10.0 10.0 10.0
9      EQUIPMENT AVAILABILITY, PERCENT -     60    70    80
   PERSONNEL PER SHIFT PER MACHINE
   11 NO. OF SUPVS -  0.05 0.05 0.05 AT $ -  25000 25000 25000
12 13 NO. OF ENGRS -  0.10 0.10 0.10 AT $ -  20000 20000 20000
14 15 NO. OF TECHN -  1.00 1.00 1.00 AT $ -  10000 10000 10000
16 POLY SILICON COST, DOLS/KG -    65  45  30
17 POLY YIELD TO RIBBON,PERCENT -    80  85  90
   SERVICES AND SUPPLIES
18     CRUCIBLE/DIE/PARTS COST PER  WEEK-  150 125 100 DOLLARS
19     POWER COST AT -  0.05 0.05 0.05 DOLLARS PER KWH
20     ENERGY TO OPERATE EQUIPMENT -    12  11  10 KW

21 22  O/H -    50  50  50 PCT OF PERS+    10  10  10 PCT OF RAW MATL COST
23  G_AND_A -    10  10  10 PERCENT OF DIRECT COST+OVERHEAD

24  PROFIT BEFORE TAX, PERCENT - 10 10 10 OF DC+O/H+G&A

  MISCELLANEOUS
25 WORKWEEK, HOURS -  168 168 168
26 CONVERSION EFFICIENCY, PERCENT -    8.00 10.00 12.00
27 ENERGY DENSITY AT AM1,KW/SQ M PEAK -     1    1    1
```

Fig. 4. List of multiple-ribbon parameters and their assigned values.

5. SENSITIVITY ANALYSIS

5.1 General

Sensitivity analysis is frequently useful in providing additional information to strengthen the case for a decision among alternatives, such as the choice between single- and multiple-ribbon growth systems. It examines conclusions in terms of their sensitivity to individual forecasts, that is, to what degree different forecasts would affect the overall conclusions.

'ABLE III. Economics of Silicon Ribbon - One Multiple-Ribbon Puller

Simulation Date and No. 03/02/75	6	7	8
Ribbons grown simultaneously	1.00	2.00	3.00
Ribbon width (cm)	2.50	3.00	5.00
Average yielded growth rate (sq m/hr)	0.02	0.08	0.39
Combined yield factor	0.56	0.68	0.81
Direct Cost (dollars/sq meter)			
Equipment capital recovery	271.70	40.06	6.25
Personnel	420.63	79.30	17.09
Polysilicon cost	81.13	30.84	12.94
Services/supplies	79.55	13.51	2.57
Subtotal:	853.02	163.71	38.85
Overhead cost (dollars/sq meter)	214.86	41.75	9.59
G&A expenses (dollars/sq meter)	106.79	20.55	4.84
Profit (dollars/sq meter)	117.47	22.60	5.33
Total cost (dollars/sq meter)	1292.13	248.61	58.62
Dollars per kw	16151.63	2486.06	488.51

In this study, sensitivity analysis is first used to further assess the advantages of single- vs multiple-ribbon growth systems. This is accomplished by testing the sensitivity of the baseline silicon sheet material cost to future advances in the previously defined three major production unit elements: processing technology, resources, and raw material costs. After the choice between single- and multiple-ribbon growth systems has been made, the components of the most sensitive production unit element are then further evaluated.

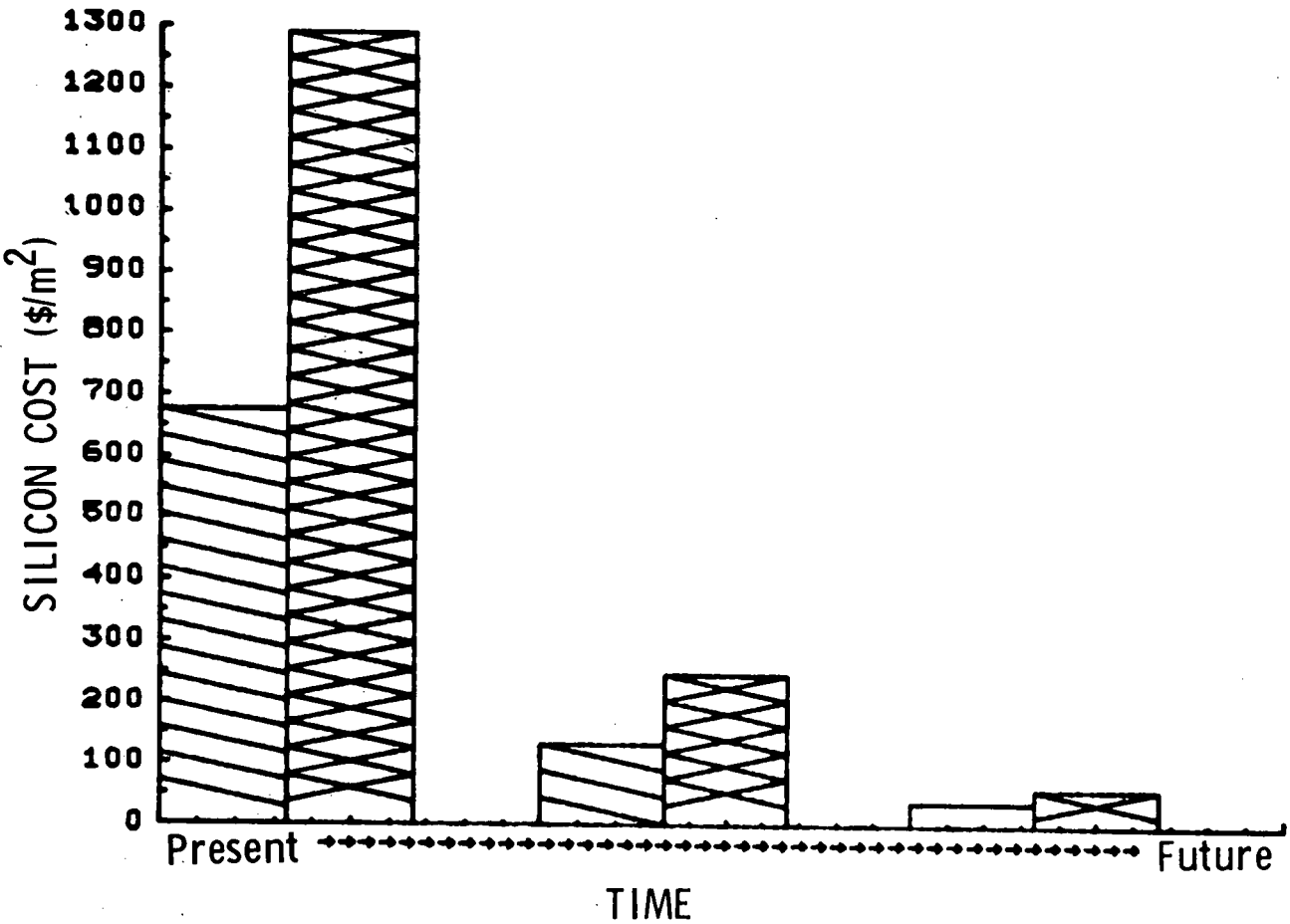

Fig. 5. Silicon sheet material cost.

The result is expected to resolve specific questions, such as (one) the effect on silicon sheet material cost if breakthroughs are made in processing technology, but all other factors, such as polycrstalline silicon cost, remain unchanged, and (two) the priority of advancing ribbon width as compared with growth rate.

5.2 Single- vs Multiple-Ribbon Growth Systems - Comparison by Major Element

To gain additional confidence in the finding for single-ribbon growth systems, the relative sensitivity of the three major production unit elements is tested through further iteration of the computer model. This is done by projecting the parameters of the components within the particular element, while keeping the remaining production unit parameters at the baseline values.

The result is shown in Fig. 6. From the baseline, or reference, on the left, the effect of advancing process technology, decreasing the amount of required capital resources, and reducing polycrystalline silicon cost is depicted. It implies that advancing processing technology is much more important, in terms of achieving a lower silicon sheet material cost, than striving to develop less costly crystal-pulling systems or inexpensive polycrystalline silicon material.

Furthermore, it suggests that low-cost silicon material objectives can be achieved by pursuing either single- or multiribbon growth. However, about twice as much effort is required to reach the low-cost objective by means of multiribbon, as compared with single-ribbon growth technology. Consequently, this examination confirms the previously reached determination favoring single-ribbon growth systems.

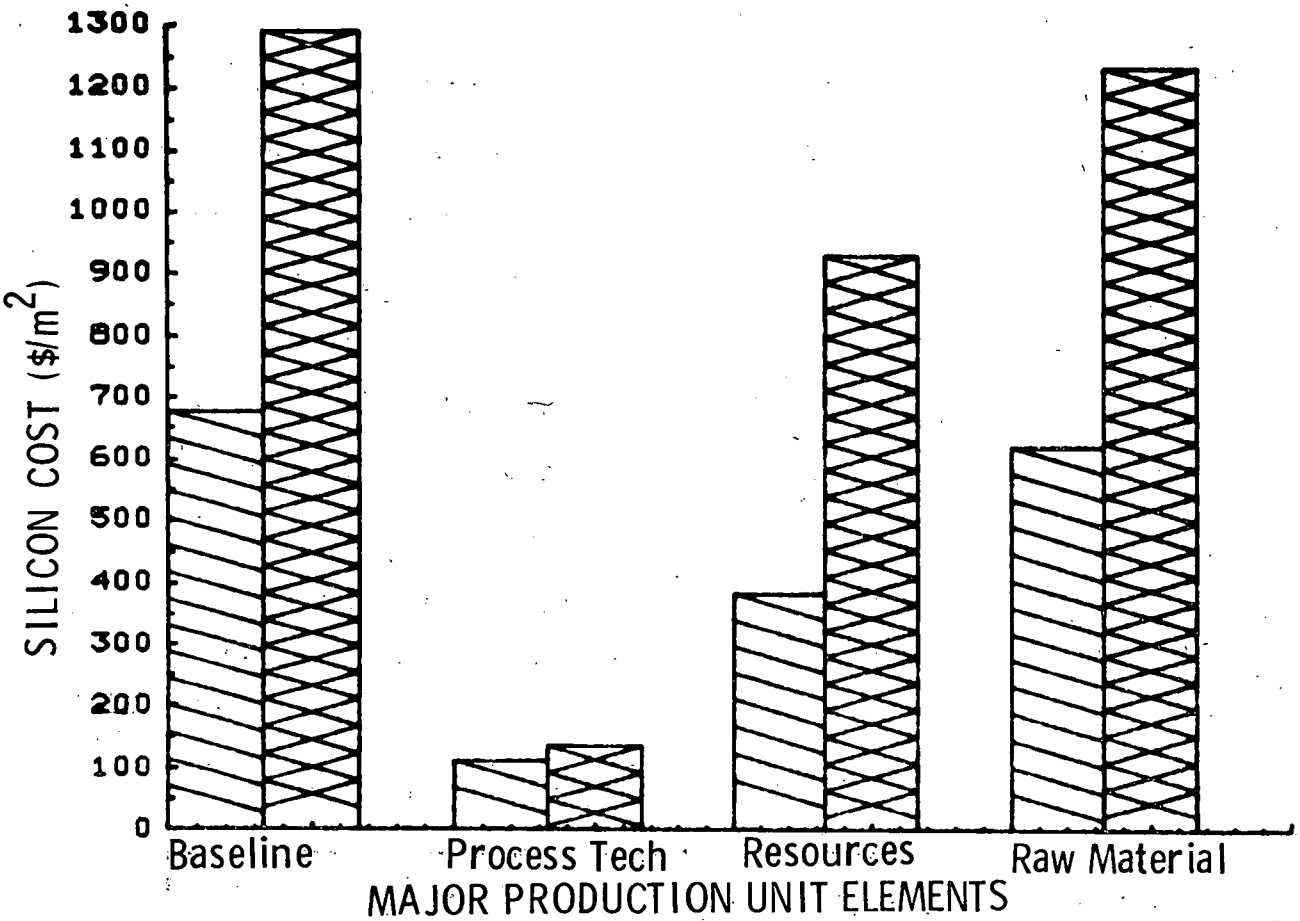

Fig. 6. Single- vs multiple-ribbon growth: comparison by major production-unit elements.

5.3 Single-Ribbon Growth Systems - Comparison of Processing Technology Components

Next, single-ribbon growth and its key element, processing technology, will be evaluated to determine where additional development effort might produce the lowest-cost silicon sheet.

The methodology consists of selecting a processing-technology component, e.g., ribbon width, and, while holding all other production unit parameters at the baseline value, iterating

the model in equal increments between the two projected limits (i.e., 2.5 to 10 cm). This is done until a sufficient number of data points for curves, such as shown in Fig. 7, can be collected.

Figure 7 suggests that increasing ribbon width from 2.5 to 10 cm has the most pronounced effect on cost, reducing silicon sheet material from \$678 to \$247/m^2, whereas the effect of reducing ribbon thickness by itself is insignificant. Improving growth rate from 30 to 50% of theoretical maximum ranks between the two, reducing cost from \$678 to \$443/m^2.

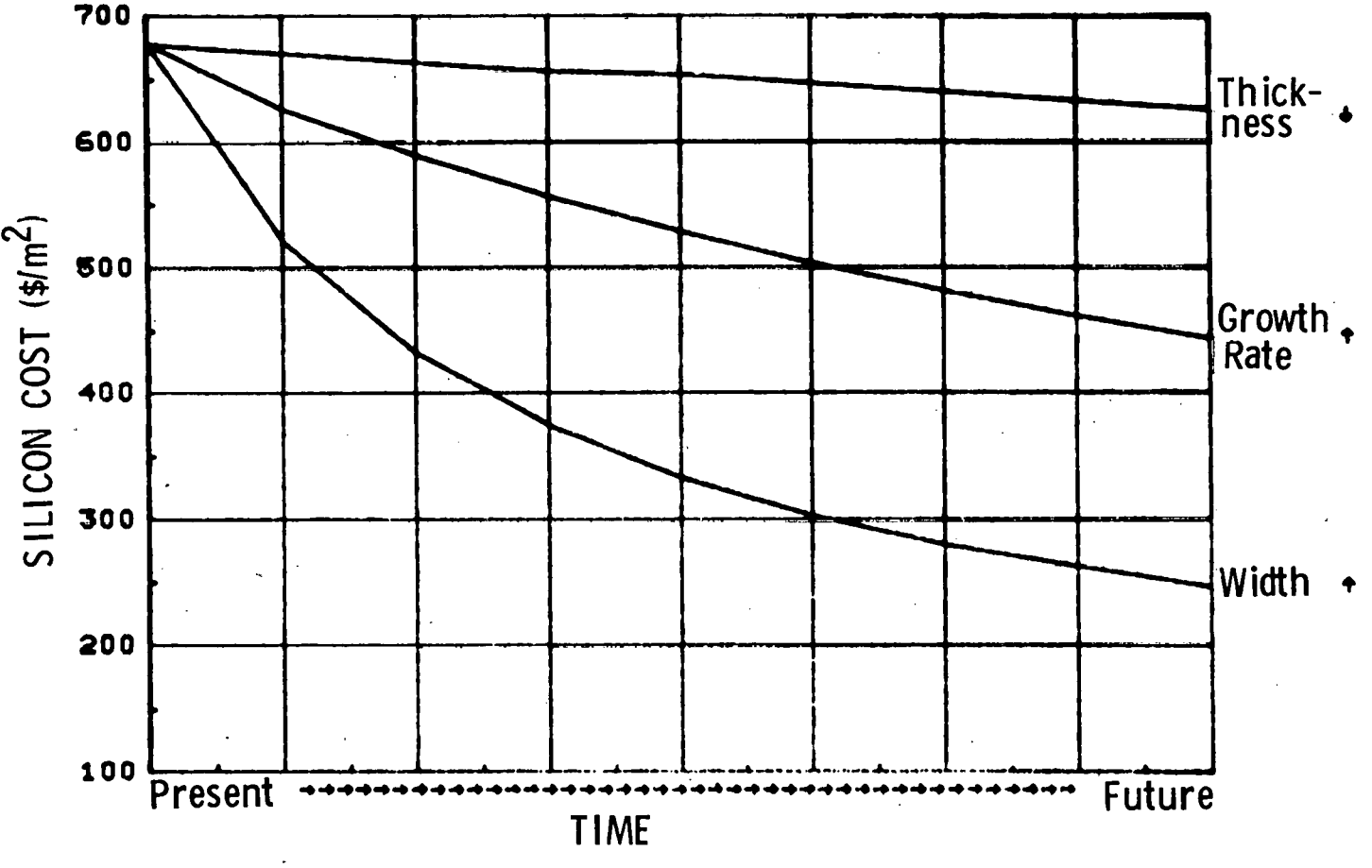

Fig. 7. Single-ribbon system: silicon sheet cost vs processing-technology parameters.

Since ribbon growth rate and ribbon thickness are related, Figure 8 compares the potential of their combined improvement, a reduction from \$678 to \$292/m^2. However, this figure is still higher than \$247/m^2, which resulted from increasing ribbon width from 2.5 to 10 cm. The combined improvement of all parameters within this production unit element yields silicon sheet material cost at \$112/m^2.

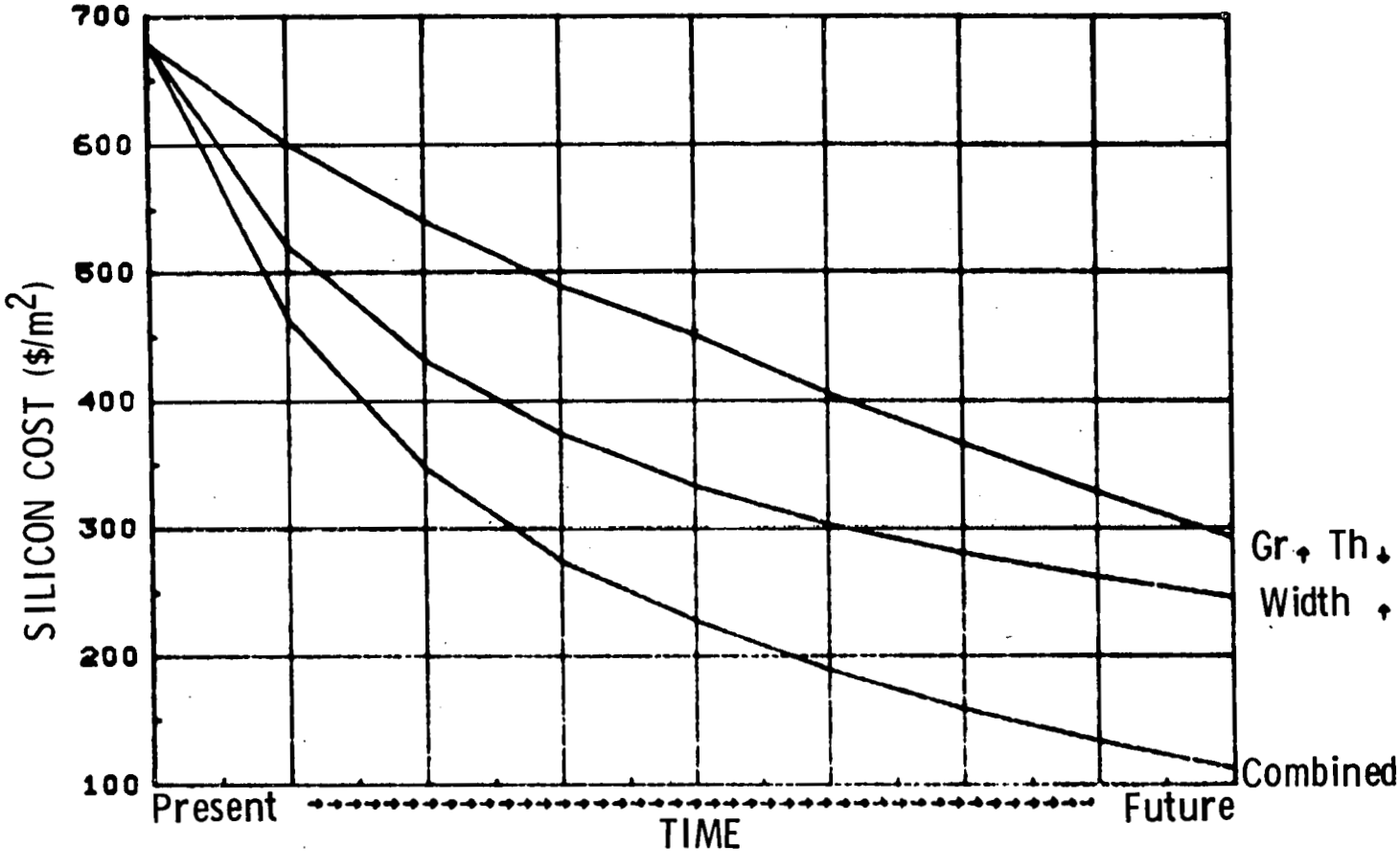

Fig. 8. Single-ribbon system: silicon sheet cost vs combined processing-technology parameters.

Additional perspective is provided in Figure 9, where silicon sheet material cost vs width is presented. It should be noted that increasing ribbon width from 2.5 to 5 cm, a near-term objective, will reduce sheet material cost from $\$678/m^2$ to $\$390/m^2$, or by almost a factor of two. Doubling ribbon width again from 5 to 10 cm will further lower material cost to $\$247/m^2$.

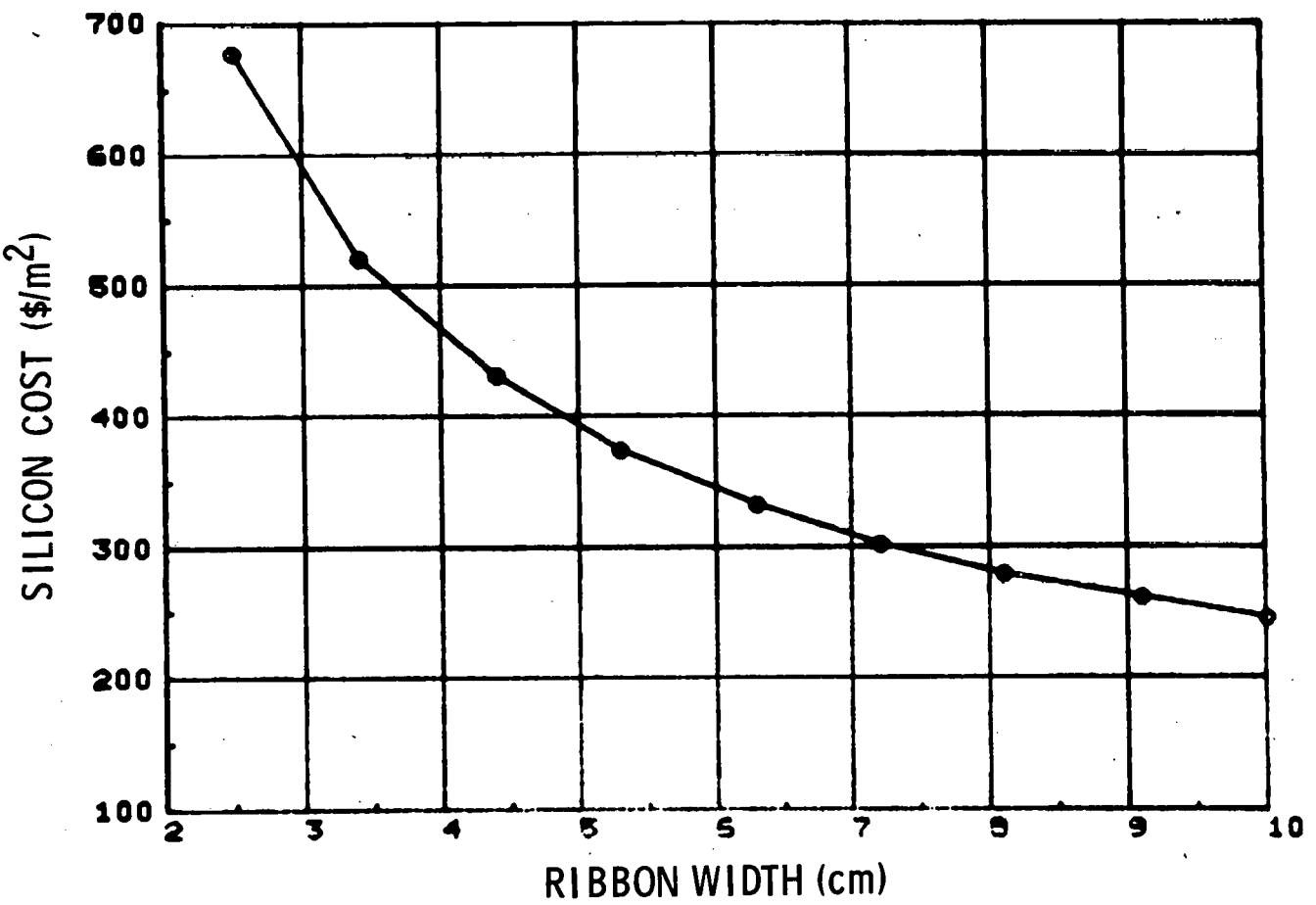

Fig. 9. Single-ribbon system: silicon sheet cost vs ribbon width.

Figure 10 presents material cost vs growth rate and shows that increasing growth rate from our baseline value of 1.5 m/hr, or 30% of theoretical maximum, to the projected 50% (1.8 m/hr), without simultaneously reducing ribbon thickness, decreases material cost from \$678 to \$443/m^2, or about 35%. Advancing both growth rate and thickness capability to the projected limits will decrease silicon material cost to \$292/m^2, or a factor of two. Accordingly, the recommendation for future effort here is to advance proficiency in both areas simultaneously, as this is more readily accomplished than pursuing only one of the items to a practical limit.

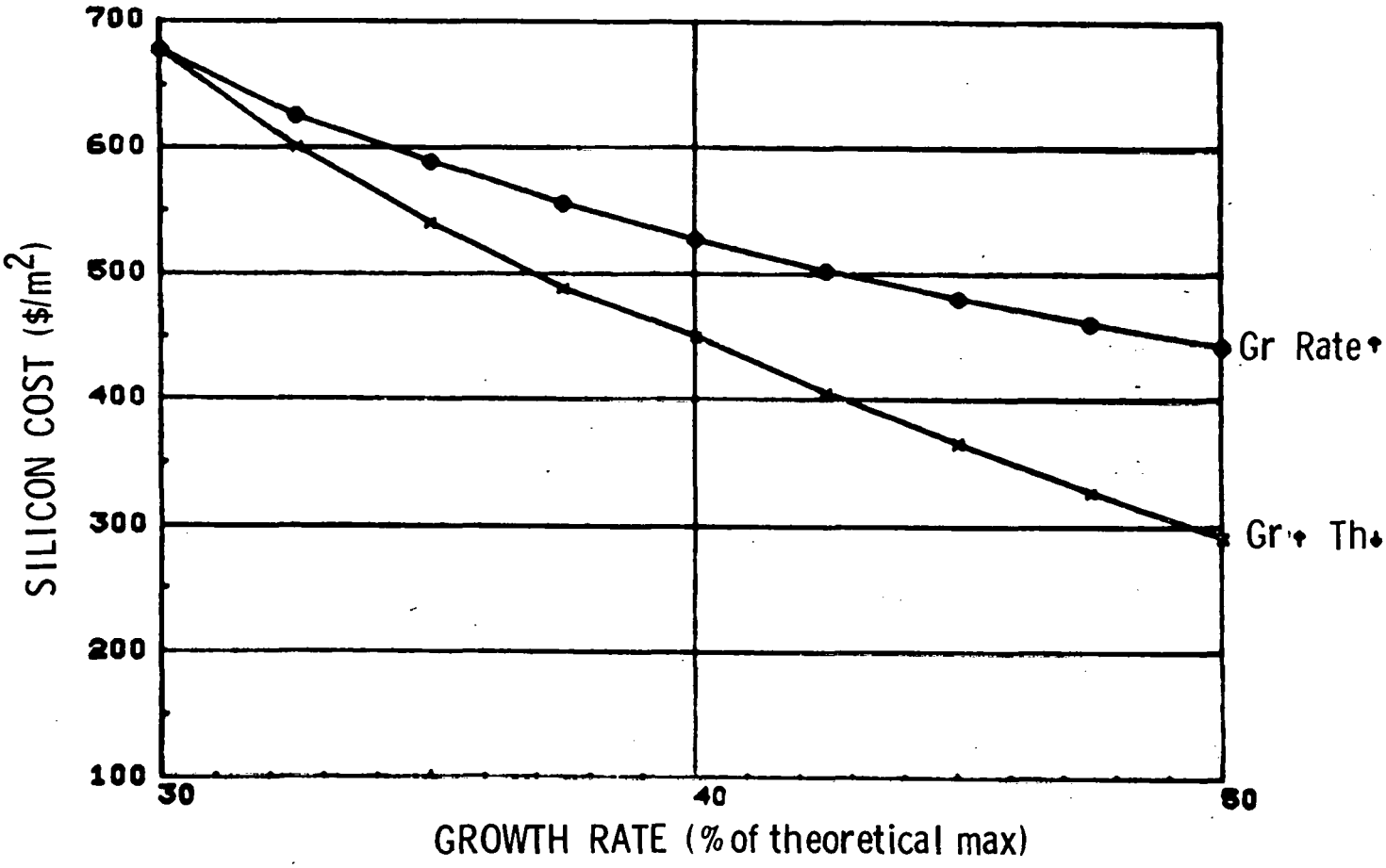

Fig. 10. Single-ribbon system: silicon sheet cost vs growth rate.

6. CONCLUSIONS

Technology projection and sensitivity analysis suggest that single-ribbon growth systems offer the best potential for achieving low-cost silicon sheet material within the shortest period of time. Such systems must be highly reliable, be capable of near unattended growth, and feature automatic melt replenishment.

Processing-technology improvements, such as

- o increasing ribbon width
- o speeding up the growth rate
- o decreasing ribbon thickness

are the key elements for reducing the cost of silicon sheet material. Such tasks should be pursued in that order to minimize sheet material cost. One interesting finding is that significant reductions in sheet material cost are achievable in the near future by increasing ribbon width to 5 cm.

7. REFERENCES

1. T. F. Ciszek, J. Appl. Phys. 47, 440 (]976).

FOURTH QUARTER ACTIVITY PLAN

- Correlate die bake-out procedures with solar-cell performance.

- Continue process studies on ribbon perfection.

- Conduct growth of sample ribbons for delivery to JPL.

- Continue ribbon evaluation through solar-cell processing.

- Continue work on solar-cell performance analysis and lifetime-generation data-analysis computer programs.

- Expand ribbon-growth computer model to address other material processing steps (e.g., slicing), if technical support is received from JPL in the definition of an acceptable methodology.